Connecting the Yakima fold and thrust belt to active faults in the Puget Lowland, Washington

Richard J. Blakely,[1] Brian L. Sherrod,[2] Craig S. Weaver,[2] Ray E. Wells,[1] Alan C. Rohay,[3] Elizabeth A. Barnett,[2] and Nichole E. Knepprath[1]

Received 5 November 2010; revised 12 April 2011; accepted 4 May 2011; published 28 July 2011.

[1] High-resolution aeromagnetic surveys of the Cascade Range and Yakima fold and thrust belt (YFTB), Washington, provide insights on tectonic connections between forearc and back-arc regions of the Cascadia convergent margin. Magnetic surveys were measured at a nominal altitude of 250 m above terrain and along flight lines spaced 400 m apart. Upper crustal rocks in this region have diverse magnetic properties, ranging from highly magnetic rocks of the Miocene Columbia River Basalt Group to weakly magnetic sedimentary rocks of various ages. These distinctive magnetic properties permit mapping of important faults and folds from exposures to covered areas. Magnetic lineaments correspond with mapped Quaternary faults and with scarps identified in lidar (light detection and ranging) topographic data and aerial photography. A two-dimensional model of the northwest striking Umtanum Ridge fault zone, based on magnetic and gravity data and constrained by geologic mapping and three deep wells, suggests that thrust faults extend through the Tertiary section and into underlying pre-Tertiary basement. Excavation of two trenches across a prominent scarp at the base of Umtanum Ridge uncovered evidence for bending moment faulting possibly caused by a blind thrust. Using aeromagnetic, gravity, and paleoseismic evidence, we postulate possible tectonic connections between the YFTB in eastern Washington and active faults of the Puget Lowland. We suggest that faults and folds of Umtanum Ridge extend northwestward through the Cascade Range and merge with the Southern Whidbey Island and Seattle faults near Snoqualmie Pass 35 km east of Seattle. Recent earthquakes ($M_W \leq 5.3$) suggest that this confluence of faults may be seismically active today.

Citation: Blakely, R. J., B. L. Sherrod, C. S. Weaver, R. E. Wells, A. C. Rohay, E. A. Barnett, and N. E. Knepprath (2011), Connecting the Yakima fold and thrust belt to active faults in the Puget Lowland, Washington, *J. Geophys. Res.*, *116*, B07105, doi:10.1029/2010JB008091.

1. Introduction

[2] The Cascadia convergent margin (northern California, Oregon, Washington, and British Columbia) is a region of profound tectonism and magmatism, ultimately caused by oblique subduction of the Juan de Fuca plate beneath North America (Figure 1). The Pacific plate, moving northwestward ~50 mm/y relative to North America, establishes dextral shear across the Juan de Fuca plate and western North America [*Atwater*, 1970; *DeMets et al.*, 1994]. Most of the Pacific-North America relative motion is accommodated by the Juan de Fuca spreading center and Cascadia subduction zone, but the remaining 20 to 25 percent is distributed across Oregon and Washington [*McCaffrey et al.*, 2007]. Oregon is rotating clockwise at about 1°/Ma, squeezing Washington against a slower-moving Canadian buttress [*Wells et al.*, 1998; *McCaffrey et al.*, 2007]. Most people in this region live in the seismically active forearc lowland, consisting of the Puget Lowland in Washington, Willamette Valley in Oregon, and Fraser Lowland in British Columbia.

[3] In the Puget Lowland, a complex system of east-west and northwest trending faults (Figure 2) accommodates 4.4 ± 0.3 mm/yr of permanent north-south shortening [*Wells et al.*, 1998; *Mazzotti et al.*, 2002; *McCaffrey et al.*, 2007]. Numerous paleoseismic studies [*Nelson et al.*, 2003; *Johnson et al.*, 2004a; *Sherrod et al.*, 2004; *Kelsey et al.*, 2004; *Sherrod et al.*, 2008] demonstrate that Puget Lowland faults produced earthquakes as large as M_W 7 in Holocene time, and a diffuse pattern of modern-day earthquakes (Figure 2) shows that many of these faults likely remain active today. Puget Lowland faults are largely concealed by young glacial deposits, water, and urban development, and much of what we know about their mapped location and three-dimensional

[1]U.S. Geological Survey, Menlo Park, California, USA.
[2]U.S. Geological Survey at Department of Earth and Space Sciences, University of Washington, Seattle, Washington, USA.
[3]Environmental Characterization and Risk Assessment Group, Pacific Northwest National Laboratory, Richland, Washington, USA.

0148-0227/11/2010JB008091

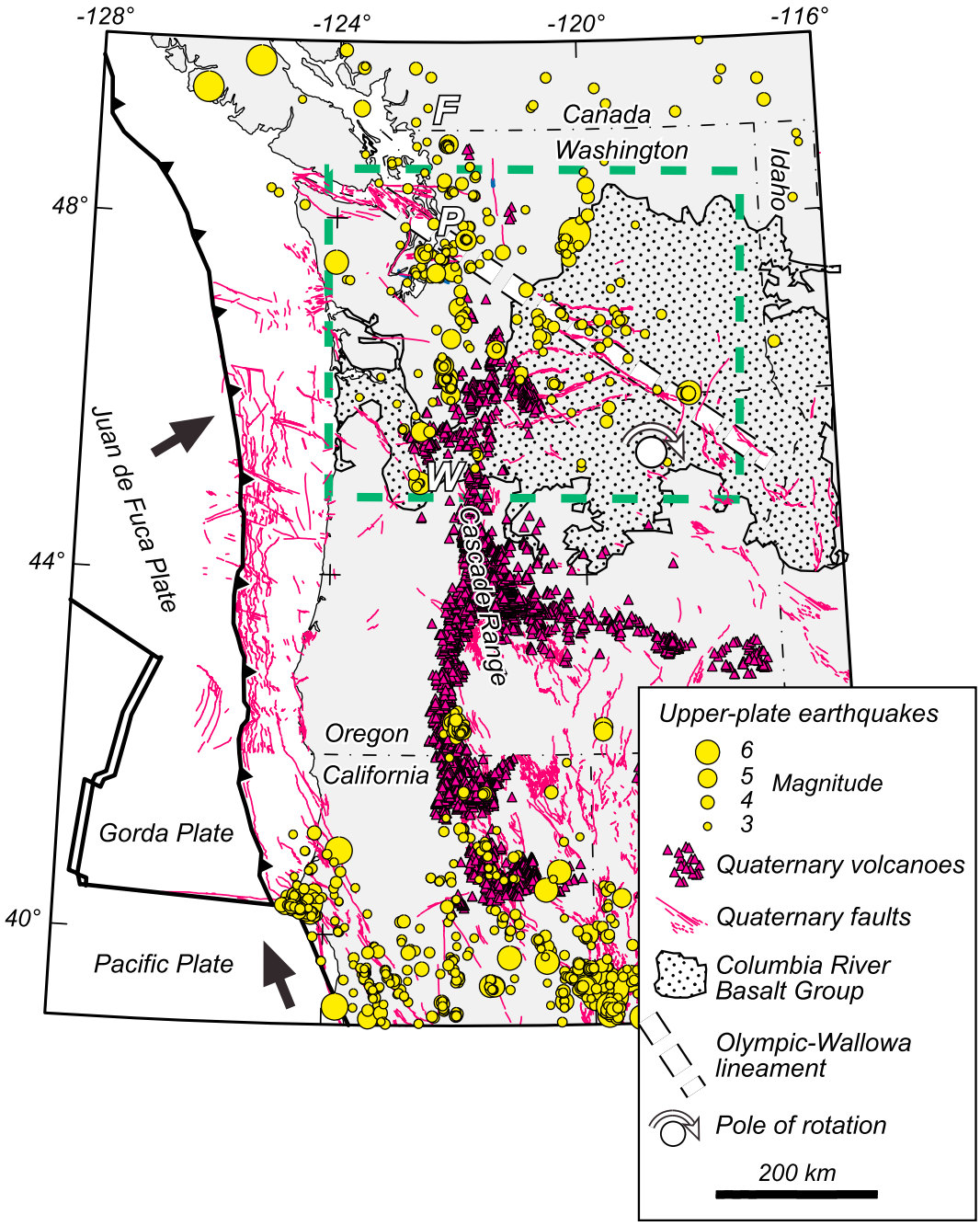

Figure 1. Tectonic and magmatic setting of the Pacific Northwest. Red lines are faults from U.S. Geological Survey Quaternary fault database (http://earthquake.usgs.gov/hazards/qfaults). Quaternary volcanoes from *Guffanti and Weaver* [1988]. Earthquake locations and magnitudes from the Pacific Northwest Seismic Network and historic records, as compiled by Katie Keranen (written communication, 2009). Olympic Wallowa lineament as described by *Raisz* [1945]. Green dashed rectangle shows area of Figure 2. F, Fraser Lowland; P, Puget Lowland; W, Willamette Valley. Pole of rotation is for Oregon Coast Range domain relative to North America, 1.02° Myr^{-1} [*McCaffrey et al.*, 2007].

framework has come from geophysical investigations [e.g., *Johnson et al.*, 1994, 1996; *Brocher et al.*, 2001; *Blakely et al.*, 2002; *Pratt et al.*, 1997].

[4] As its name implies, the Yakima fold and thrust belt (YFTB), situated on the east side of the Cascade Range, is also a region of profound deformation [e.g., *Reidel et al.*, 1989a, 1989b]. Columbia River Basalt Group (CRBG; 17.5–6.0 Ma) and suprabasalt sedimentary deposits record Late Miocene and Pliocene faulting and folding in the YFTB. Paleoseismic investigations show that the YFTB continued to evolve in Quaternary time [*West et al.*, 1996; *Campbell and Bentley*, 1981; *Repasky et al.*, 2009], and moderate-sized

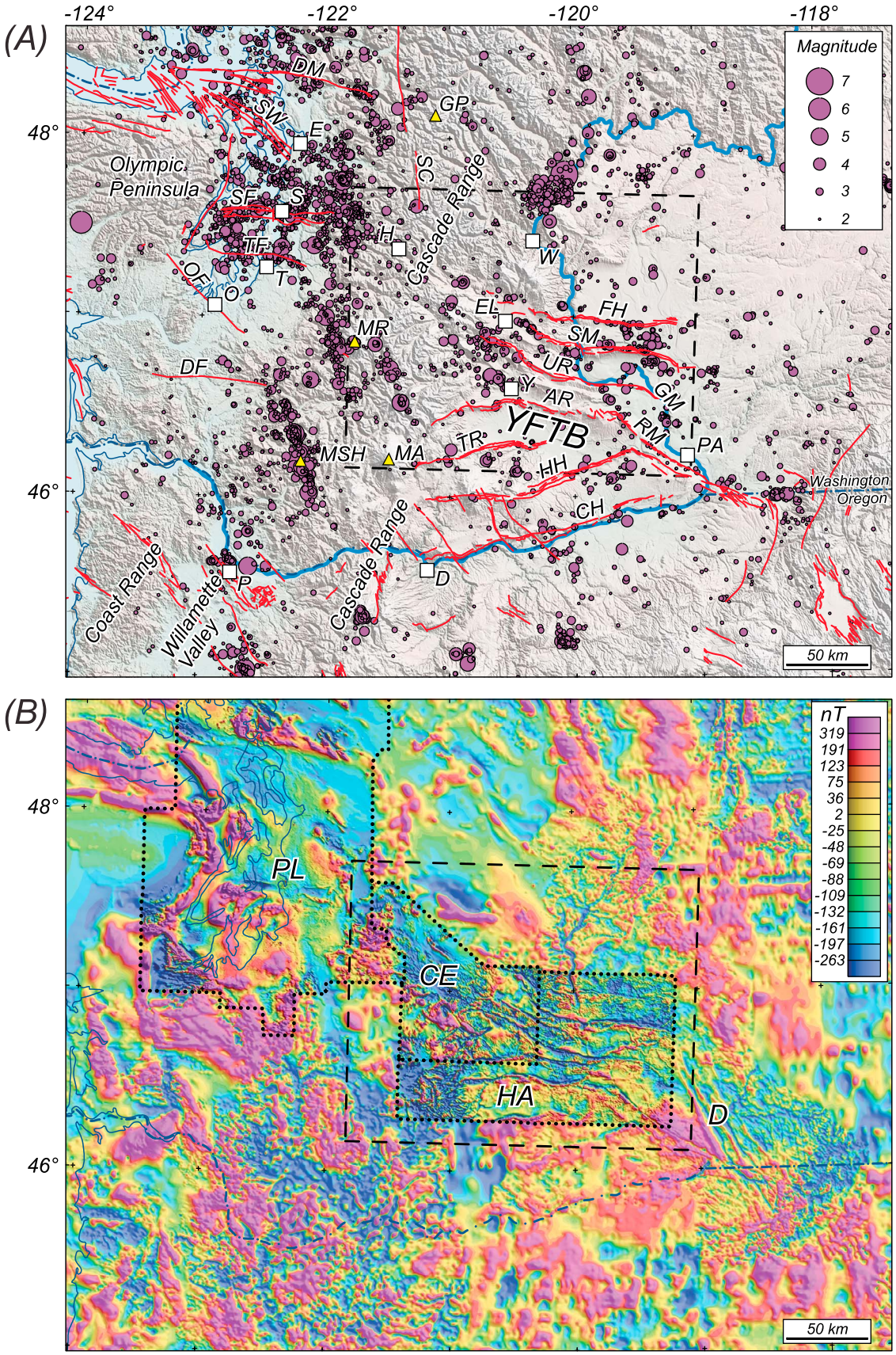
(A)
-124°
-122°
-120°
-118°
48°
46°
Magnitude
7
6
5
4
3
2
DM
SW
E
GP
Olympic
Peninsula
SF
S
SC
Cascade Range
H
W
TF
T
OF
O
EL
FH
MR
SM
DF
UR
Y
AR
GM
YFTB
RM
TR
MSH
MA
HH
PA
Washington
Oregon
CH
Coast Range
Willamette
Valley
P
D
Cascade Range
50 km
(B)
48°
46°
nT
319
191
123
75
36
2
-25
-48
-69
-88
-109
-132
-161
-197
-263
PL
CE
HA
D
50 km

Figure 2

earthquakes in the region suggest that some of these structures remain active today (Figure 2).

[5] If extended southeastward along strike, important Holocene faults in the Puget Lowland coincide with Quaternary faults of the YFTB. Structures linking the two regions would cross the Cascade Range along the Olympic-Wallowa lineament (OWL, Figure 1), a topographic and structural lineament extending from the Olympic Peninsula in Washington to the Wallowa Mountains in Oregon [*Raisz*, 1945; *Hooper and Conrey*, 1989]. *McCaffrey et al.* [2000, 2007] argued from GPS measurements that the OWL is the primary locus of deformation resulting from clockwise rotation of Oregon and Washington relative to stationary North America. In this paper, we use (1) new aeromagnetic and paleoseismic data and (2) existing gravity and lidar (light detection and ranging) data to investigate the possibility that Puget Lowland and YFTB structures are kinematically linked, and we attempt to map the linking structures through the intervening Cascade Range of Washington.

2. Geologic and Structural Setting

[6] Paleomagnetic [e.g., *Simpson and Cox*, 1977; *Wells*, 1990; *Wells et al.*, 1998] and global positioning system (GPS) measurements [e.g., *Mazzotti et al.*, 2002; *McCaffrey et al.*, 2000, 2007] show that western Oregon and Washington are rotating clockwise with respect to stable North America at a rate of 0.4 to 1.0° Myr^{-1} and have been doing so at approximately steady rates for the last 10–15 Ma. This broad rotation relative to stable North America within British Columbia produces horizontal strain that varies in direction and magnitude throughout Cascadia. The region of Washington immediately west of the Cascade Range, for example, is translating northward at a rate of 4.2 to 6.2 mm/yr relative to stable North America, whereas regions immediately east of the Cascade Range are translating northeastward at ~1/3 that rate [*McCaffrey et al.*, 2007]. *McCaffrey et al.* [2007] modeled Pacific Northwest GPS velocities with strain accommodated between rigid blocks. The YFTB constitutes two block boundaries in their model, together accommodating ~3 mm/yr of northeast shortening.

[7] It should be noted that the various maps employ two published fault databases. When discussing mapped geology, we show *all* faults regardless of age, as mapped at 1:100,000 scale by the Department of Natural Resources, Washington State. When the purpose of the map is to describe geologic hazards, we only show faults currently considered to have been active in Quaternary time (http://earthquake.usgs.gov/hazards/qfaults). The latter database is essentially a subset of the former, and captions indicate which database was employed.

2.1. Puget Lowland

[8] North-south compression in westernmost Washington is accommodated in part by a system of east-west and northwest striking crustal faults crossing the Puget Lowland (Figure 2). Many of these faults have been active in Holocene time and are spatially and structurally associated with large structural basins and uplifts observable in gravity and seismic data. Three Holocene faults are particularly important to subsequent discussion: (1) The east striking Seattle fault is a north verging thrust fault that, over the course of the last 40 m.y., has lifted its hanging wall up and over the Seattle basin to the north, now a 9 to 10 km deep basin filled with Oligocene and younger sedimentary rocks and glacial deposits [*Johnson et al.*, 1994; *Pratt et al.*, 1997; *Blakely et al.*, 2002; *Brocher et al.*, 2001, 2004; *ten Brink et al.*, 2002]. (2) The Tacoma fault, along the southern margin of the Seattle uplift, is a south verging thrust fault serving as the structural contact between the uplift and the Tacoma basin to the south [*Johnson et al.*, 2004b; *Sherrod et al.*, 2004]. (3) The northwest striking Southern Whidbey Island fault, extending from near Vancouver Island to east of Seattle, accommodates right-lateral oblique displacement and forms the southwestern structural margin of the Everett basin [*Johnson et al.*, 1996; *Sherrod et al.*, 2008]. The Seattle and Southern Whidbey Island faults, if continued eastward along strike, merge near Snoqualmie Pass (Figure 2, label H) 35 km east of Seattle.

[9] Holocene fault scarps of the Puget Lowland are each associated with linear magnetic anomalies that reflect the juxtaposition of lithologic units of differing magnetic properties. This association has proved useful in mapping Puget Lowland faults where concealed beneath Pleistocene glacial deposits, water, and urban development [e.g., *Blakely et al.*, 2002, 2009; *Sherrod et al.*, 2008]. With the advent of airborne lidar methods during the past decade, numerous topographic scarps were discovered throughout the Puget Lowland. These scarps often offset Pleistocene and younger surfaces and lie parallel and very near to linear magnetic anomalies [e.g., *Sherrod et al.*, 2008]. Paleoseismic excavations, targeted at lidar-identified scarps, show a rich history of Holocene earthquake activity throughout the Puget Lowland [e.g.,

Figure 2. (a) Earthquakes and Quaternary faults of western and central Washington and northern Oregon. Earthquake locations and magnitudes provided by Katie Keranen (written communication, 2009). YFTB, Yakima fold and thrust belt. Red lines are Quaternary faults from U.S. Geological Survey Quaternary fault database (http://earthquake.usgs.gov/hazards/qfaults). DM, Devils Mt.; SW, Southern Whidbey Island; SF, Seattle; TF, Tacoma; OF, Olympia; DF, Doty; SC, Straight Creek; FH, Frenchman Hills; SM, Saddle Mountains; UR, Umtanum Ridge; AR, Ahtanum Ridge; RM, Rattlesnake Mountain; TR, Toppenish Ridge; HH, Horse Heaven Hills; CH, Columbia Hills; GM, Gable Mountain. Cities and towns indicated by white boxes: E, Everett; S, Seattle; T, Tacoma; O, Olympia; P, Portland; D, The Dalles; PA, Pasco; Y, Yakima; EL, Ellensburg; W, Wenatchee; H, Hyak (Snoqualmie Pass). Yellow triangles are major volcanoes: GP, Glacier Peak; Mount Rainier; MSH, Mount St. Helens; MA, Mount Adams. Black dashed rectangle is location of Figures 4, 6–10. (b) Magnetic anomalies of central Washington and northern Oregon [*Finn et al.*, 1989; *Roberts et al.*, 1997]. Dotted lines indicate boundaries of high-resolution aeromagnetic data used in subsequent figures: PL, Puget Lowland magnetic survey [*Blakely et al.*, 1999]; CE, Cle Elum survey; HA, Hanford survey. Label D indicates north-northwest striking magnetic anomalies interpreted as dikes by *Swanson et al.* [1979] and discussed in text.

Nelson et al., 2003; *Sherrod et al.*, 2008; *Johnson et al.*, 2004a]. In particular, the Seattle, Tacoma, and Southern Whidbey Island faults each produced multiple M_W 6.5–7.0 earthquakes in Holocene time.

2.2. Yakima Fold and Thrust Belt

[10] Flows of the CRBG (Figure 3) dominate the geologic landscape of the YFTB. CRBG flood basalts erupted from vents and fissures in southeastern Washington and northeastern Oregon 17.5 Ma to 6.0 Ma (Figure 4). Together they filled a volume of 174,000 km^3, covered an area of about 163,700 km^2 [*Tolan et al.*, 1989, 2009], and in some cases flowed all the way to the Pacific Ocean [*Beeson et al.*, 1989; *Wells et al.*, 2009]. By far the greatest pulse of CRBG extrusion occurred 17.0 to 15.6 Ma, with eruption of the Grande Ronde Basalt: approximately 120 individual flows that together comprise 148,600 km^3 of basaltic lava [*Reidel et al.*, 1989b]. The Grande Ronde Basalt is the most prevalent CRBG formation in our study area. Eruptions of Grande Ronde Basalt spanned four polarity intervals (Figure 3), at least two of which (R_2 and N_2) are exposed in our study area (Figure 4).

[11] North-south compression of the YFTB has formed a series of east-west anticlines, synclines, and associated faults more or less evenly spaced across the landscape (Figures 2 and 4). The mapped distribution of YFTB structures essentially fans out in the westward direction (Figure 2), such that the northern anticlines (Frenchman Hills, Saddle Mountains and Umtanum Ridge) are directed northwestward toward the Puget Lowland, and southern anticlines (Toppenish Ridge, Horse Heaven Hills, and Columbia Hills) are directed southwestward toward Portland, Oregon. This distribution suggests complexities in the north-south compressive strain over the course of YFTB evolution. The region now occupied by the YFTB was a focus of back-arc subsidence before, during, and after CRBG emplacement [*Reidel*, 1984, *Reidel et al.*, 1989a, 1994], and YFTB anticlines continued to evolve during this time so that the degree of folding increases with depth into CRBG stratigraphy [*Reidel*, 1984]. Deformation of CRBG also postdates its eruption and emplacement [e.g., *Mitchell and Montgomery*, 2006; *West et al.*, 1996; *Campbell and Bentley*, 1981], as discussed in the following sections.

[12] CRBG flood basalts naturally filled whatever terrain existed at the time of extrusion, but in general, each newly erupted flow formed a quasi-horizontal layer that recorded subsequent folding and faulting. This obvious point has important implications for geophysical analysis: Basalts are strongly magnetic, having induced magnetizations on the order of 0.1 to 0.5 A/m and natural remanent magnetizations of 1 to 10 A/m. Deformed CRBG flood basalts, therefore, produce distinctive magnetic anomalies that facilitate mapping and characterization of these structures. The CRBG includes both normal and reversely magnetized flows, as well as flows with transitional remanent magnetizations. CRBG flows have Koenigsberger ratios generally >10 (Figure 5), and the juxtaposition of normal and reversed flows adds complexity to the analysis of magnetic anomalies.

[13] Pre-Tertiary rocks exposed in the northern part of our study area (Figure 4) likely extend in the subsurface beneath parts of the CRBG [*Campbell*, 1989]. These basement rocks include Jurassic metamorphic and ophiolitic rocks of the Ingalls Tectonic Complex [*Dragovich et al.*, 2002] and Cretaceous granitic rocks of the Mount Stuart batholith [*Smith*, 1904; *Dragovich et al.*, 2002]. As discussed subsequently, gravity anomalies indicate the subsurface distribution of these lithologies.

[14] Continental sedimentary and volcaniclastic rocks comprise the Tertiary stratigraphy above pre-Tertiary basement and below CRBG flows, and variations in their stratigraphic thickness have important implications for both hydrocarbon exploration and earthquake hazards. Geophysical studies indicate that basement relief exceeds relief on the base of CRBG [*Saltus*, 1993; *Jarchow*, 1991], implying that YFTB deformation was underway before and continued during CRBG emplacement. If it can be shown that topography on the basement interface is spatially associated with CRBG folds and faults, this would provide a strong case that faults seen at the surface extend into the basement rather than shoaling into detachment surfaces within or at the base of CRBG. In the study area, exposures of pre-CRBG Tertiary rocks include Eocene continental sedimentary rocks of the Swauk, Manastash, Roslyn, and Chumstick Formations; and volcanic rocks of the Oligocene Ohanepecosh Formation and Miocene Fifes Peak Formation [*Tabor et al.*, 2000; *Walsh et al.*, 1987; *Stoffel et al.*, 1991; *Schuster et al.*, 1997; *Dragovich et al.*, 2002].

[15] CRBG flows are overlain and intercalated by Miocene continental sedimentary and volcaniclastic rocks of the Ellensburg Formation, which in turn is overlain by Pliocene-Miocene Ringold Formation, Pliocene Thorp Gravel, and Pleistocene outburst flood deposits [*Walsh et al.*, 1987; *Schuster et al.*, 1997; *Dragovich et al.*, 2002]. All of these post-CRBG units are deformed, including the 1 Ma to 12 ka Hanford Formation [*Repasky et al.*, 2009].

2.3. Olympic-Wallowa Lineament

[16] A regional-scale topographic lineament, extending from the Olympic Peninsula to the Wallowa Mountains, is superimposed on the tectonic magmatic framework of the Pacific Northwest (Figure 1). The origin of the Olympic-Wallowa lineament, first recognized 65 years ago by *Raisz* [1945], is still a matter of discussion. *Kienle et al.* [1977] referred to that part that crosses the central Columbia Basin as the Cle Elum-Wallula (CLEW) lineament. Within the YFTB, the OWL corresponds with the Rattlesnake Mountain and Umtanum Ridge anticlines (Figure 2). Beyond the Columbia basin, the OWL aligns with linear topographic features in pre-CRBG rocks both northwest and southeast of these anticlines [*Campbell*, 1989]. *Hooper and Conrey* [1989] envisioned the OWL as a giant megashear accommodating differential extension rates, with opening rates to the south approximately 20 percent greater than regions to the north. A differential opening rate implies shear strain along the OWL, but direct evidence of strike-slip displacement has been elusive [*Tabor et al.*, 1984; *Reidel et al.*, 1989a; *Price and Watkinson*, 1989; *Saltus*, 1993]. Moreover, dextral shear on the OWL is not evident in GPS measurements. *McCaffrey et al.* [2007] document northeast directed shortening across the OWL, decreasing in magnitude to the southeast. In their microplate model, the OWL forms a

Series	Group	Formation	Member	Isotopic Age (m. y.)	Magnetic Polarity
Miocene Upper	Columbia River Basalt Group	Saddle Mountains Basalt	Lower Monumental Member	6	N
			Ice Harbor Member	8.5	
			Basalt of Goose Island		N
			Basalt of Martindale		R
			Basalt of Basin City		N
			Buford Member		R
			Elephant Mountain Member	10.5	R,T
			Pomona Member	12	R
			Esquatzel Member		N
			Weissnefels Ridge Member		
			Basalt of Slippery Rock		N
			Basalt of Tenmile Creek		N
			Basalt of Lewiston Orchards		N
			Basalt of Cloverland		N
			Asotin Member	13	
			Basalt of Huntzinger		N
			Wilber Creek Member		
			Basalt of Lapwai		N
			Basalt of Wahluke		N
			Umatilla Member	13.5	N
			Basalt of Sillusi		N
			Basalt of Umatilla Member		N
Middle		Wanapum Basalt	Priest Rapids Member	14.5	
			Basalt of Lolo		R
			Basalt of Rosalia		R
			Roza Member		T,R
			Shumaker Creek Member		N
			Frenchman Springs Member		
			Basalt of Lyons Ferry		N
			Basalt of Sentinel Gap		N
			Basalt of Sand Hollow	15.3	N
			Basalt of Silver Falls		N,E
			Basalt of Ginkgo		E
			Basalt of Palouse Falls		E
			Eckler Mountain Member		
			Basalt of Dodge		N
			Basalt of Robinette Mountain		N
			Vantage Horizon		
Lower		Grande Ronde Basalt (Prineville Basalt)	Sentinel Bluffs Member	15.6	N_2
			Slack Canyon Member		
			Field Springs Member		
			Winter Water Member		
			Umtanum Member		
			Ortley Member		
			Armstrong Canyon Member		
			Meyer Ridge Member		R_2
			Grouse Creek Member		
			Wapshilla Ridge Member		
			Mt. Horrible Member		
		Picture Gorge Basalt	China Creek Member		N_1
			Downey Gulch Member		
			Center Creek Member		R_1
			Rogersburg Member		
			Teepee Butte Member		
			Buckhorn Springs Member	16.5	
		Imnaha Basalt			R_1
					T
					N_0
				17.5	R_0

Figure 3. Stratigraphic elements of the CRBG [*Reidel et al.*, 1989b]. N, R, T, E refer to normal, reversed, transitional, and east directed magnetizations, respectively.

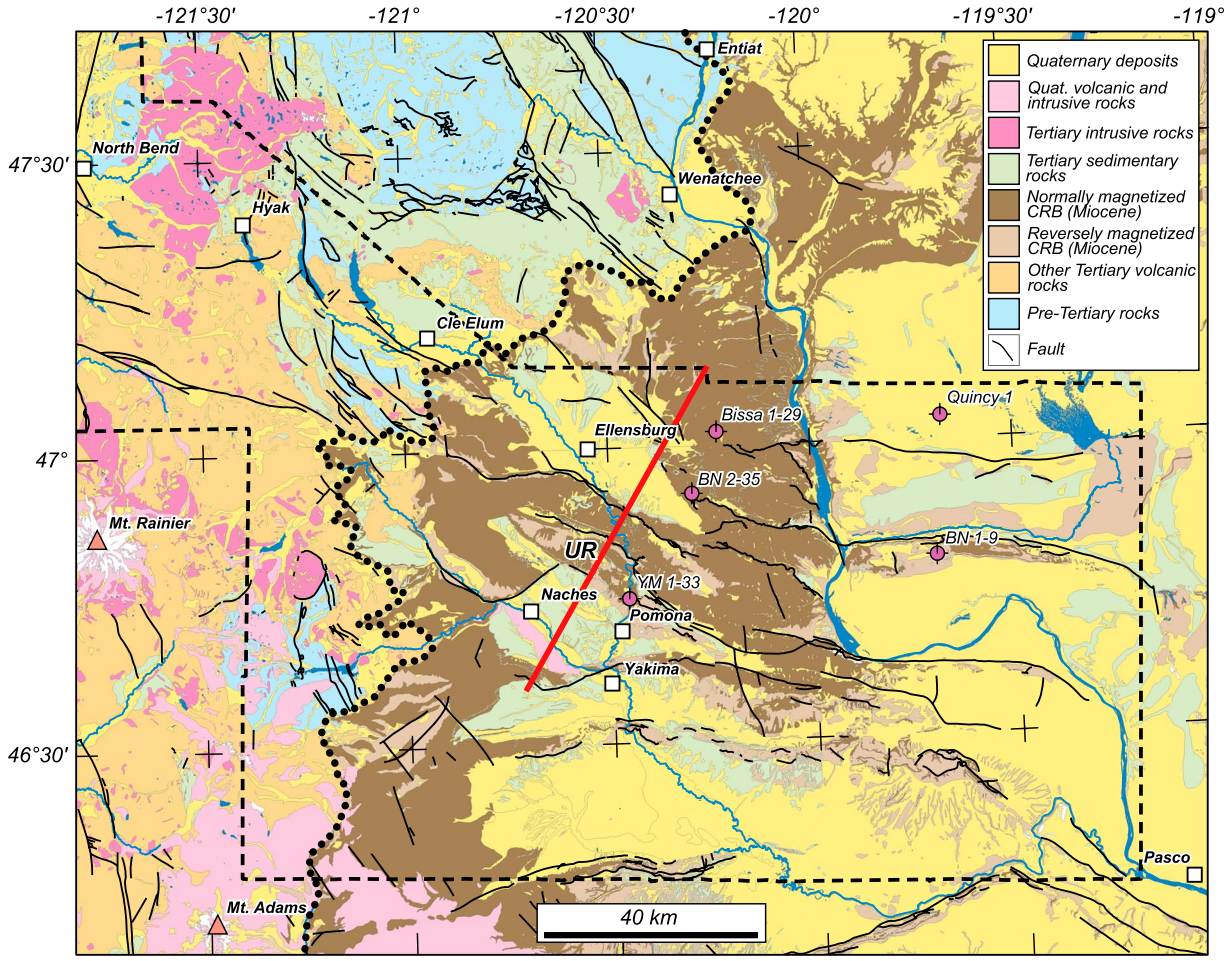

Figure 4. Generalized geology of the YFTB and surrounding regions, simplified from *Walsh et al.* [1987], *Schuster et al.* [1997], *Stoffel et al.* [1991], and *Dragovich et al.* [2002]. Black solid lines are faults of all types and ages, modified from the above references. Note that these faults differ from those shown on Figures 1, 2, 6, 7, 9, 10, and 20, which reflect Quaternary faults only (http://earthquake.usgs.gov/hazards/qfaults). Black dotted line indicates western limit of exposed Columbia River Basalt Group. Black dashed line shows extent of high-resolution aeromagnetic surveys discussed in text. Red line is location of gravity and magnetic model discussed in text and shown in Figure 20. Magenta symbols are deep exploratory boreholes [*Reidel et al.*, 1989b] discussed in text. UR, Umtanum Ridge.

boundary between YFTB blocks, with poles of rotation in Idaho near the southeastward projection of the OWL.

3. Geophysical Analysis

3.1. Aeromagnetic Anomalies

[17] Two high-resolution airborne magnetic surveys acquired by the U.S. Geological Survey in 2008 and 2009 (Figure 6) help improve our understanding of the YFTB and possible links to neighboring tectonic structures. The surveys were acquired by separate geophysical companies working under contract to the USGS. Both surveys measured the total magnetic field at a nominal altitude of 250 m above ground or as near to the ground as safely possible. Topographic relief in some parts of the study area necessitated higher flight altitudes; nevertheless, 87 percent of the area was flown at altitudes less than 500 m above ground, and 99.4 percent at altitudes less than 1000 m. Flight lines were directed east-west in the western survey and north-south in the eastern survey. In each survey, flight lines and perpendicular tie lines were spaced 400 m and 4 km apart, respectively. Stationary magnetometers were operated continuously during data acquisition in order to monitor and subsequently correct for transient magnetic fields. Total field measurements were reduced to total field anomaly values by subtraction of the International Geomagnetic Reference Field, updated to the date of flying. The two new surveys were gridded at 100 m spacing, then merged with each other and with a third high-resolution magnetic survey flown over the Puget Lowland in 1997 [*Blakely et al.*, 1999]. Each of the three surveys overlaps its neighbors by small amounts, which facilitated the merging procedure. Merging was accomplished by determining a suture path within the overlap regions. Mismatches at each point of the suture path were then corrected within circular regions surrounding each point. Figure 6 shows merged total field magnetic anomalies reduced to the pole. Together, the three aeromagnetic surveys extend from the YFTB to the Puget

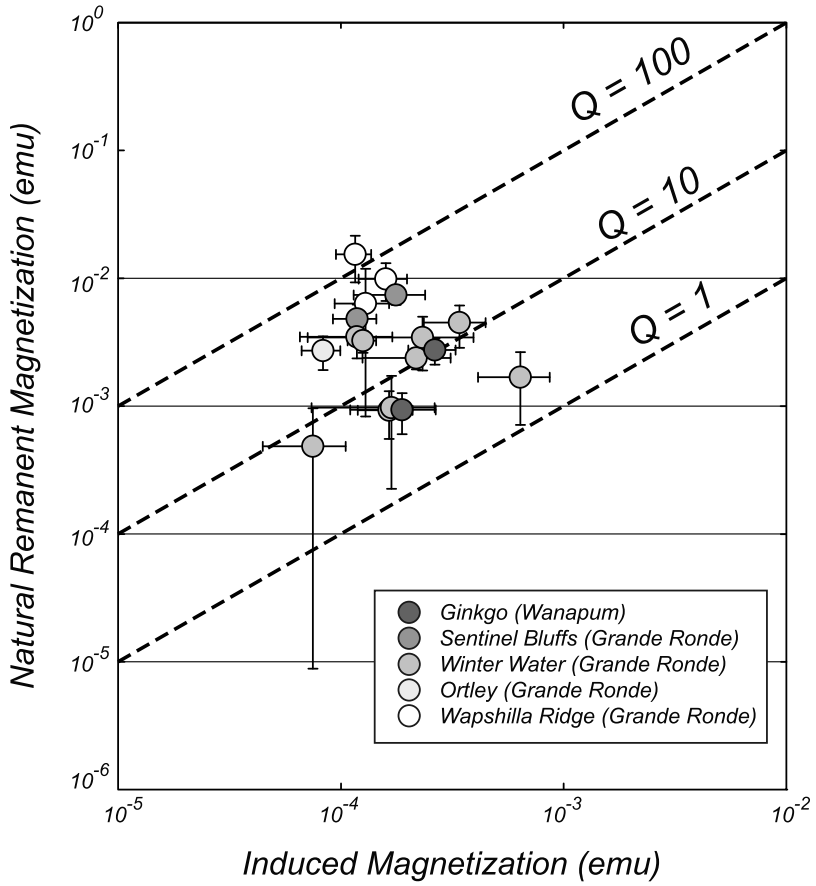

Figure 5. Koenigsberger ratios (Q) for a set of CRBG rocks. Data provided by Jon Hagstrum (written communication, 2009).

Lowland and include the intervening region where the OWL crosses the Cascade Range.

[18] The new airborne magnetic surveys cover the entire northern parts of the YFTB, including the Frenchman Hills, Saddle Mountains, Umtanum Ridge, Ahtanum Ridge, and Toppenish Ridge anticlines, and their possible extensions into the Cascade Range (Figure 6). The surveys are underlain by rocks with diverse magnetic properties, ranging from highly magnetic CRBG, with both normal and reversed remanent magnetization, to essentially nonmagnetic sedimentary rocks. Flows of the CRBG produce a distinctive, short-wavelength pattern of magnetic anomalies, making it possible to trace the western extent of CRBG volcanic units (Figure 6, dotted line). Each faulted anticline within the CRBG produces a clear aeromagnetic lineament, which is expected considering the high magnetizations of CRBG rocks. Of particular note in Figure 6 is the close alignment of distinct magnetic gradients with each Quaternary fault cataloged by the U.S. Geological Survey (http://earthquake.usgs.gov/hazards/qfaults). Additional linear anomalies lie west of CRBG exposures with trends similar to Quaternary faults mapped within the CRBG.

[19] Figure 2a shows significant topographic relief associated with YFTB anticlines and synclines, and we should consider the possibility that linear magnetic anomalies in Figure 6 are caused simply by topographic effects in this highly magnetic terrain. To investigate this possibility, we calculated the magnetic anomalies that would be observed on a horizontal surface immediately above the highest topography assuming uniformly magnetized crust and using the method of *Parker* [1972]. These calculated anomalies showed little resemblance to observed anomalies when continued upward to the same level. We conclude that long-wavelength topographic anomalies are not significant in this area, and that observed anomalies instead are caused mostly by subsurface magnetic sources (e.g., faulted contacts, folded layers, changes in magnetic polarity, etc.).

[20] Figure 7 shows magnetic anomalies filtered in order to emphasize shallow magnetic sources. These anomalies were calculated by analytically continuing the original magnetic field (Figure 6) 50 m upward, then subtracting that result from the original field. This two-step procedure is equivalent to a discrete vertical derivative, which emphasizes magnetic anomalies caused by shallow sources at the expense of anomalies originating from deeper sources [*Blakely*, 1995]. Regions of distinctly different magnetic character are apparent in Figure 7. For example, it is easy to distinguish near-surface CRBG from less magnetic lithologies, and it is apparent from this pattern that CRBG does not extend west of its geologically mapped surface exposures (Figure 7, dotted line).

[21] Figure 7 dramatically illuminates the major folds and thrusts of the YFTB, with distinct linear anomalies closely aligned along each mapped Quaternary fault (http://earthquake.usgs.gov/hazards/qfaults). A number of linear anomalies with similar trend lie northwest of the mapped faults and

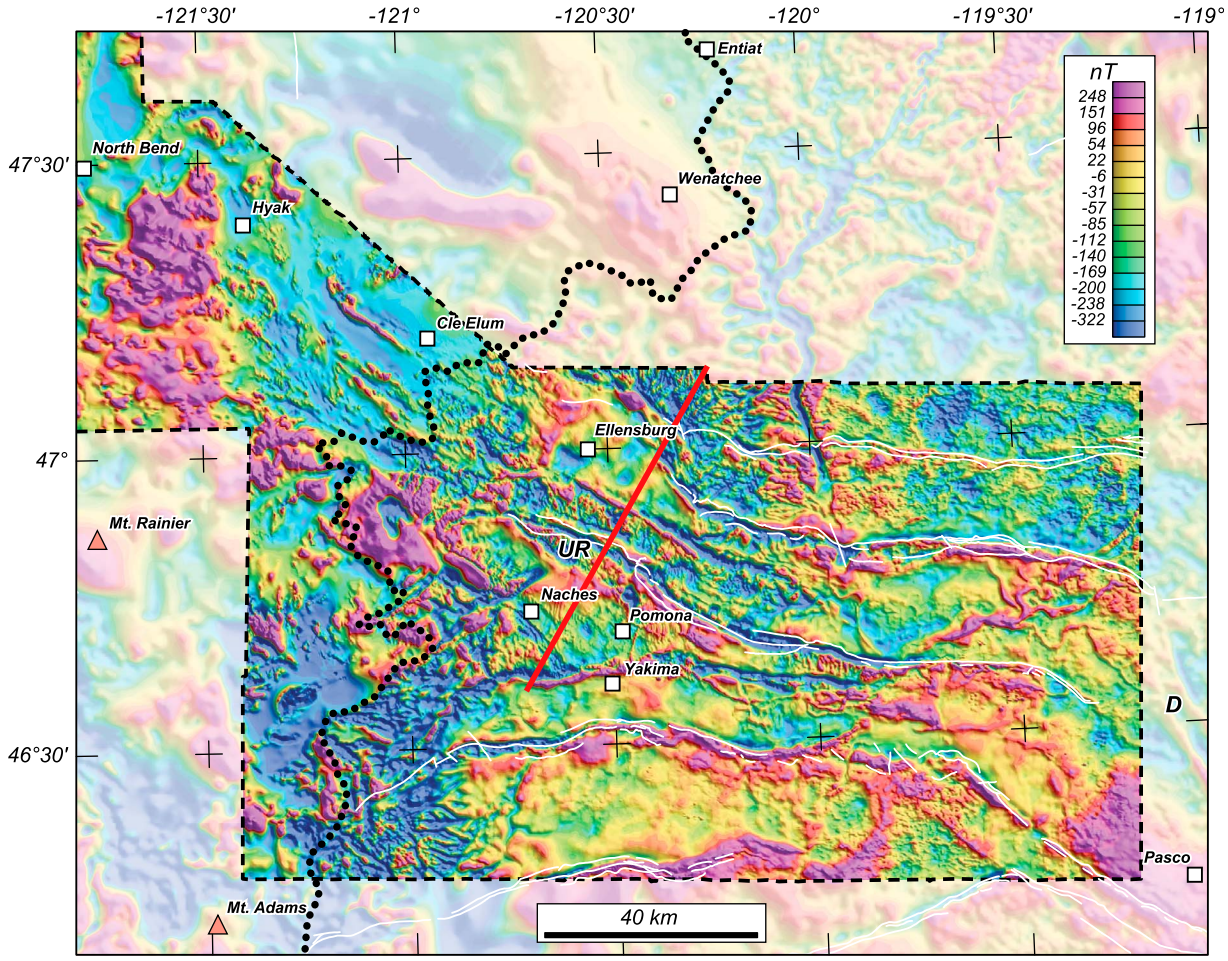

Figure 6. Total field magnetic anomalies of the YFTB and surrounding regions. Brightly colored region shows magnetic anomalies from a merge of three high-resolution surveys (see Figure 2b for survey identification). Anomalies transformed to the north magnetic pole. Subdued background colors show magnetic anomalies from a statewide compilation [*Finn et al.*, 1989] reduced to pole. White lines are Quaternary faults from the U.S. Geological Survey Quaternary fault database (http://earthquake.usgs.gov/hazards/qfaults). Note that these faults differ from those shown in Figure 4, which show faults of all ages. Dotted line shows mapped western extent of CRBG. Red line is location of magnetic and gravity profile (Figure 20). Label D indicates north-northwest striking magnetic anomalies interpreted as dikes [*Swanson et al.*, 1979]. See Figure 2 for description of other labels.

beyond exposed CRBG. In some cases, these linear anomalies can be explained by mapped lithologic contacts. For example, the northwest striking magnetic lineament immediately west of Cle Elum (Figures 6 and 7) overlies a fault-bounded sliver of Eocene volcanic rocks [*Walsh et al.*, 1987; *Dragovich et al.*, 2002]. Other northwest striking lineaments, however, are not associated with mapped features and apparently originate from lithologic contacts concealed by younger rocks and surficial deposits.

[22] We employed a method described by *Phillips et al.* [2007] to assist in mapping aeromagnetic lineaments. Black lines (made up of intersecting black dots) in Figure 8 indicate the locations of magnetic contacts calculated directly from the mathematical curvature of total field magnetic anomalies. Although this method is entirely objective, it does involve several simplifying assumptions, the most significant being the assumption that faults dip vertically. Violations of this assumption, as surely must occur in this thrust fault environment, tend to shift the calculated boundaries in the direction of dip, but these shifts are small and barely observable at the scale of Figure 8.

[23] Using original magnetic anomalies (Figure 6) and derivative products (Figures 7 and 8), we interpreted magnetic contacts that to us appear to be most significant (Figure 9). We were as objective as possible in our selection process, focusing on both anomaly amplitude and sharpness of gradients, and recognizing that a certain amount of subjectivity was unavoidable. We tended to favor magnetic lineaments that fall on or near faults already identified as active in Quaternary time (http://earthquake.usgs.gov/hazards/qfaults), as well as lineaments that lie on or near *any* fault, regardless of age, mapped by the Department of Natural Resources, State of Washington.

[24] Numerous magnetic contacts are located directly along mapped Quaternary faults. Indeed, all geologically mapped Quaternary faults correlate with magnetic contacts,

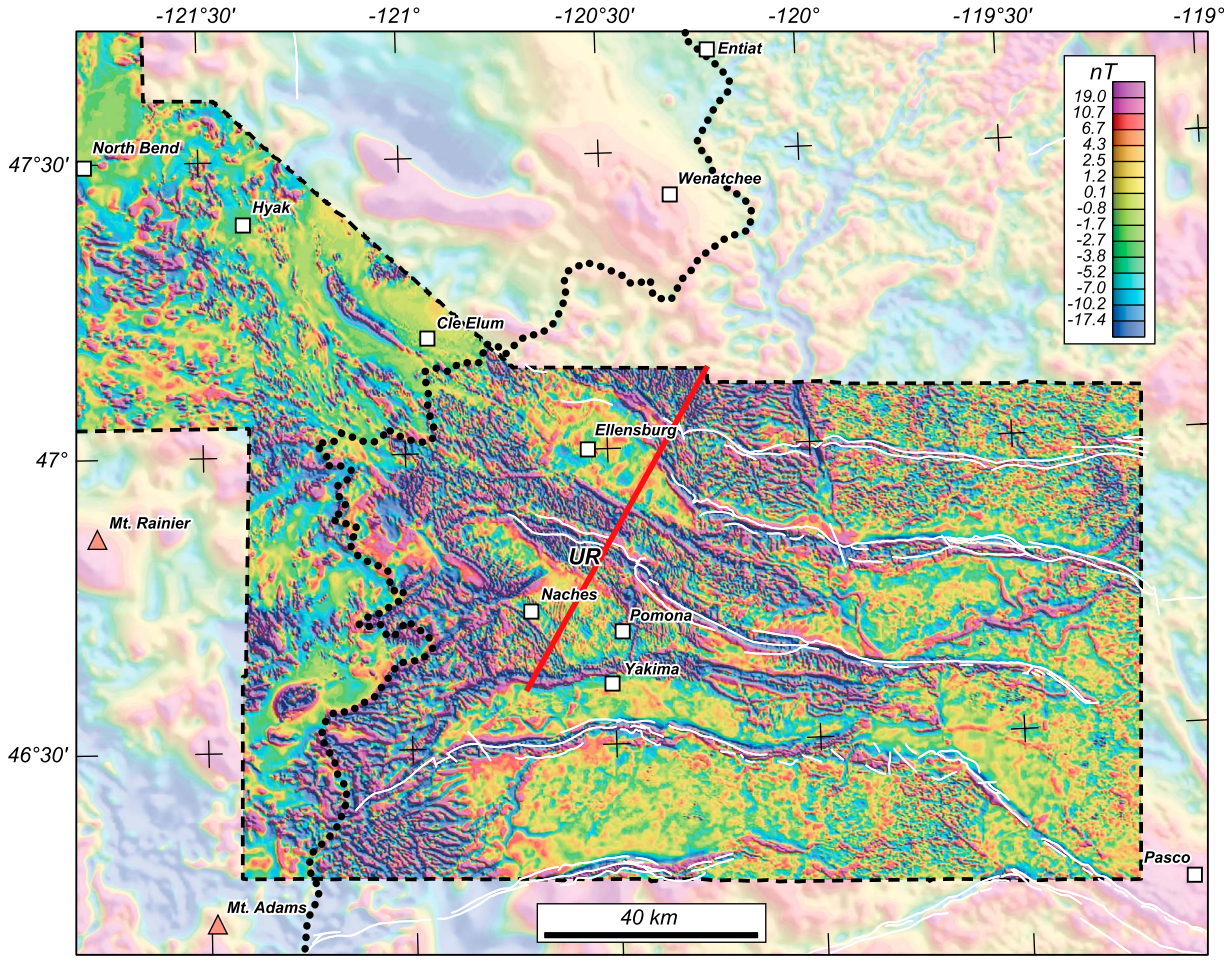

Figure 7. Residual magnetic anomalies of the YFTB and surrounding regions. Magnetic anomalies of Figure 6 filtered in order to emphasize shallow magnetic sources, as described in text. White lines are Quaternary faults (see Figure 6). See Figure 6 for description of other items.

suggesting that some of the other highlighted magnetic lineaments in Figure 9 are caused by concealed Quaternary faults. A good example is the sharp, west-northwest striking magnetic lineament immediately south of Ellensburg, evident in Figures 6–8. This magnetic lineament follows Manastash Ridge, a faulted anticline in CRBG. Manastash Ridge does not appear as a fault on Figures 6 and 7 (white lines) because it has not been recognized as active in Quaternary time (http://earthquake.usgs.gov/hazards/qfaults). On the other hand, we do believe the Manastash Ridge magnetic lineament reflects a significant structure, and thus it does appear on Figure 9.

[25] Within CRBG terrane, faults often bound regions with distinct magnetic character, and Umtanum Ridge is a good example. This fault bounded ridge displays characteristic, short-wavelength magnetic anomalies distinctly different from regions immediately south and north of the bounding faults (Figure 7). In the case of Umtanum Ridge, the change in character across the faults is caused by the relative depth of CRBG: basalts exposed at Umtanum Ridge are faulted to deeper levels both south and north of the ridge.

3.2. Analysis of Gravity Anomalies

[26] Regional gravity data provide additional subsurface information. Our gravity database includes published data from *Finn et al.* [1991], supplemented with high-quality proprietary data acquired in the 1980s for hydrocarbon exploration. Gravity measurements were reduced to isostatic residual gravity anomalies [*Simpson et al.*, 1986] using standard procedures [*Blakely*, 1995]. Station spacing is highly variable in the study area, ranging from 400 m along many roads and trails to greater than 10 km in some areas. In general, station density is adequate for regional-scale interpretations, especially over the YFTB.

[27] Figure 10 shows isostatic residual gravity anomalies of the study area. *Saltus* [1993] described regional gravity anomalies in this area, and we use his nomenclature and labeling scheme where possible. The dominant gravity anomaly in the region lies north of Cle Elum (Figure 10, label PT). This positive anomaly overlies exposures of pre-Tertiary rocks of the Wenatchee block: the Cretaceous Mount Stuart batholith, the Jurassic Ingalls Tectonic Complex, and other Mesozoic metamorphic rocks (Figure 4) [*Dragovich et al.*, 2002]. The spatial association of this

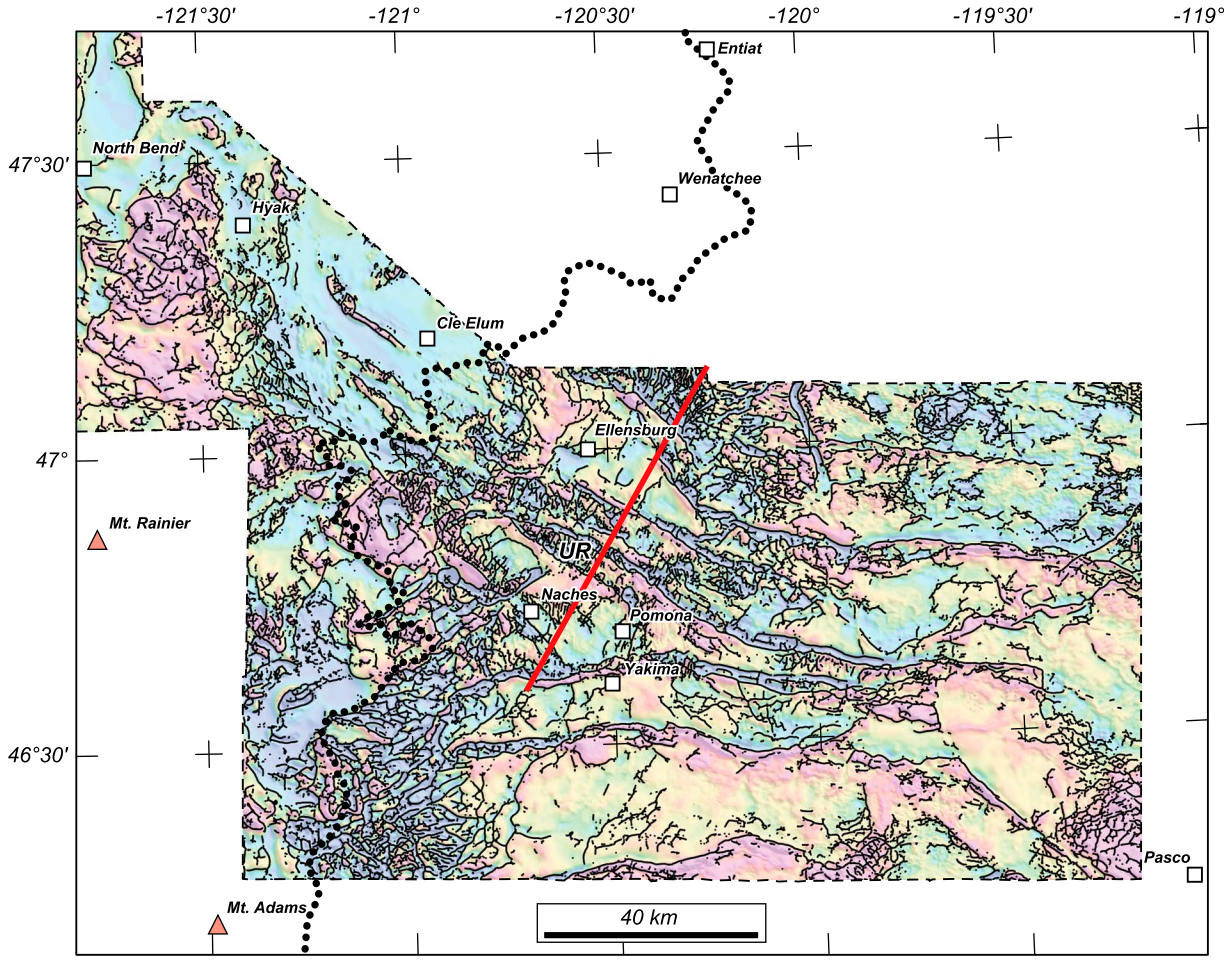

Figure 8. Magnetic contacts of the YFTB and surrounding regions. Black dots indicate contacts between lithologies of differing magnetic properties, as determined from curvature analysis [*Phillips et al.*, 2007] and applied to the magnetic anomalies of Figure 6. Background colors are magnetic anomalies, reduced to pole as shown in Figure 6.

anomaly with pre-Tertiary exposures suggests that the entire high-amplitude anomaly is caused by similar, mostly concealed pre-Tertiary basement.

[28] Other gravity anomalies shown in Figure 10 include the central gravity high (CH), the Yakima gravity low (YL), the Pasco gravity low (PL), and the Grand Coulee gravity low (GCL). These anomalies have been interpreted in two rather different ways: *Catchings and Mooney* [1988] modeled Bouguer gravity values along a 260 km long, northeast striking seismic refraction and wide-angle reflection transect and concluded that the central gravity high is caused by a thickened section of lower crust, possibly the result of crustal underplating from mantle sources. *Saltus* [1993], on the other hand, used isostatic residual gravity anomalies to construct a three-dimensional model of the entire Columbia basin. *Saltus* [1993] assumed that CRBG is uniformly dense in this area and that CRBG thickness is given by published isopach estimates [*Reidel et al.*, 1989b]. Thus defined, *Saltus* [1993] then calculated the gravitational effects of CRBG and assumed the remaining gravity anomaly was caused primarily by variations in the thickness of sub-CRBG Tertiary sedimentary rocks. His model predicted, for example, that the Yakima gravity low overlies a sub-CRBG basin filled with >5 km of Tertiary sedimentary rocks, whereas the central gravity high is caused by thinning of Tertiary sedimentary rocks, in some places being completely absent. *Saltus* [1993] also recognized that the gravity anomalies could be caused by lateral variations in basement density, as might be caused by the presence of silicic intrusions. These disparate interpretations [*Catchings and Mooney*, 1988; *Saltus*, 1993] have led to spirited debate [e.g., *Catchings and Saltus*, 1994] that, in our view, has not been fully resolved.

[29] In our interpretation, the Wenatchee block is bisected by a south-southeast trending gravity trough (Figure 10, label CG) coincident with the Chiwaukum structural low, a down-faulted block filled with Eocene and Oligocene continental sedimentary rocks [*Gresens et al.*, 1981; *Cheney and Hayman*, 2009; *Haugerud and Tabor*, 2009]. The gravity trough extends southward and broadens beneath the CRBG, separating the western Wenatchee block from the central gravity high (Figure 10, label CH). The Yakima low (YL) and the Ellensburg basin could be related in part to Eocene deformation prior to emplacement of the CRBG. Within the YFTB, the central gravity high has lower amplitude highs and lows trending roughly east-west. Some of the highs

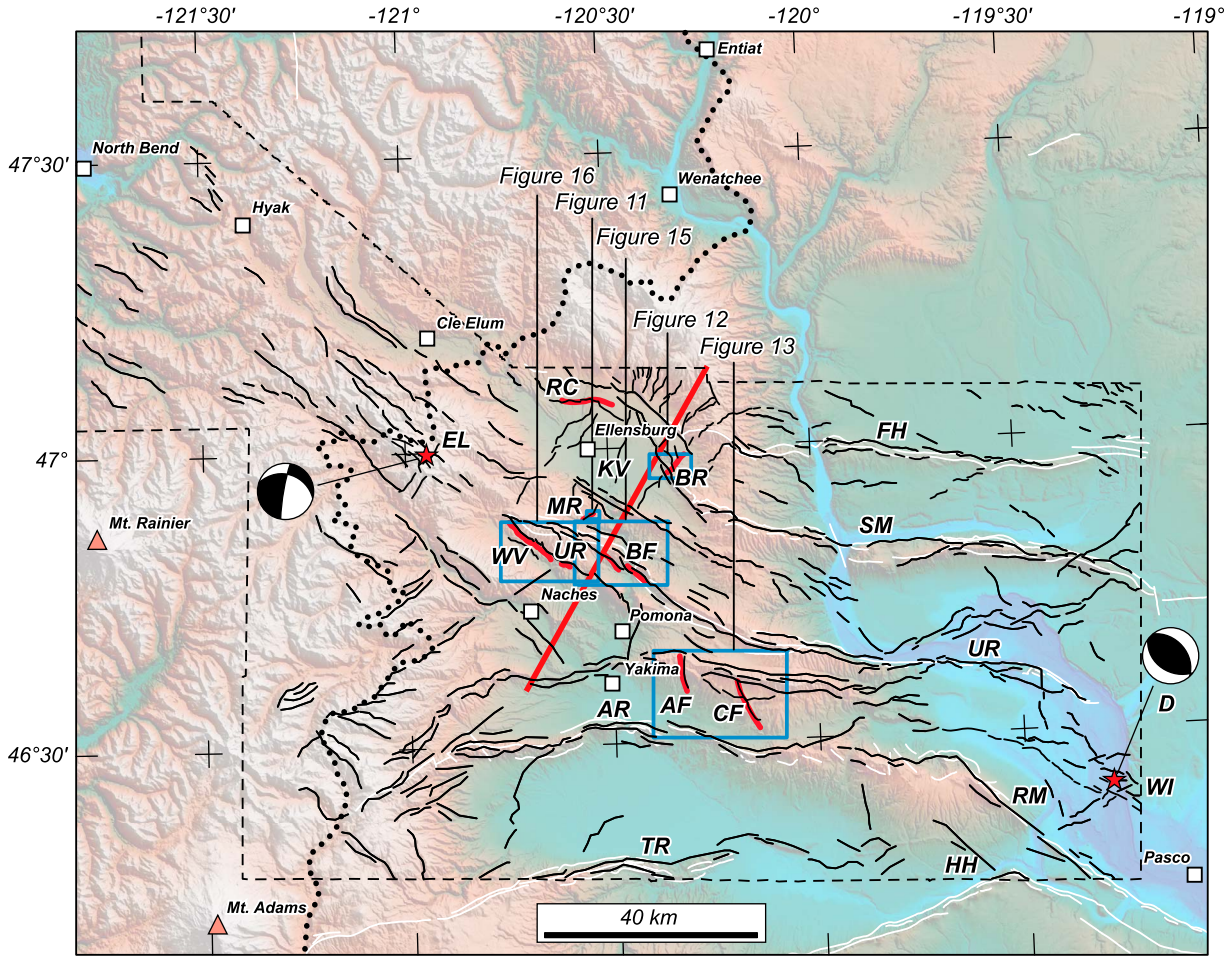

Figure 9. Solid black lines indicate significant magnetic contacts from Figure 8 used in subsequent analysis. White lines are Quaternary faults (see Figure 6). Black dashed line indicates boundary of high-quality aeromagnetic data, to which this analysis was restricted. Red lines are scarps discussed in text: MR, Manastash Ridge fault; RC, Reecer Creek fault; WV, Wenas Valley fault; BR, Boylston Ridge fault; BF, Burbank fault; AF, Artesian fault; CF, Coyote Spring fault. Red stars and accompanying focal mechanisms refer to two regions of recent seismic activity: EL, a M_W 3.8 earthquake near Ellensburg in March 2010; WI, a swarm of >1000 microearthquakes at Wooded Island in 2009 (Pacific Northwest Seismic Network, http://www.pnsn.org/welcome.html, 2010). Other locations: UR, Umtanum Ridge; KV, Kittitas Valley. See Figure 6 for description of other items.

coincide with post-CRBG structures inferred from aeromagnetic data and suggest basement involvement. Large-amplitude, north-northwest striking magnetic anomalies, interpreted as CRBG feeder dikes [*Swanson et al.*, 1979], are visible in older aeromagnetic data (Figures 2b and 6, label D) and appear to be restricted to the adjacent Pasco low (Figure 10, label PL).

[30] A northwest striking gravity lineament (Figure 10, white dotted lines) extends across the entire study area. West of the central gravity high, this lineament is manifested as a positive gravity anomaly that in part overlies basement exposures south of Cle Elum. Thus, we interpret this anomaly as being caused by shallow basement, as also noted by *Saltus* [1993]. East of the central gravity high, the lineament is characterized as a gradient between the central gravity high and the Pasco gravity low. *Saltus* [1993] suggested that the northwest striking gradient east of the central gravity high may reflect dextral shear, as proposed by *Hooper and Conrey* [1989]. However, the western margin of the central gravity high is not offset by this northwest striking structure, suggesting that dextral shear, if it exists, is older than the basement uplift that causes the central gravity high [*Saltus*, 1993]. Analysis of GPS data suggests that the OWL in the YFTB is largely a zone of northeast directed shortening, although some dextral slip is permissible in the Cascade Range [*McCaffrey et al.*, 2007].

4. Geomorphology and Lidar Topography

[31] Using magnetic anomalies and magnetic lineaments as general guides, we searched available lidar topographic data and airborne photography for geomorphic evidence of past surface ruptures. Lidar data were collected using high-resolution airborne laser swath mapping techniques and are available from two sources: the Puget Sound Lidar Consortium (http://pugetsoundlidar.ess.washington.edu; resolution =

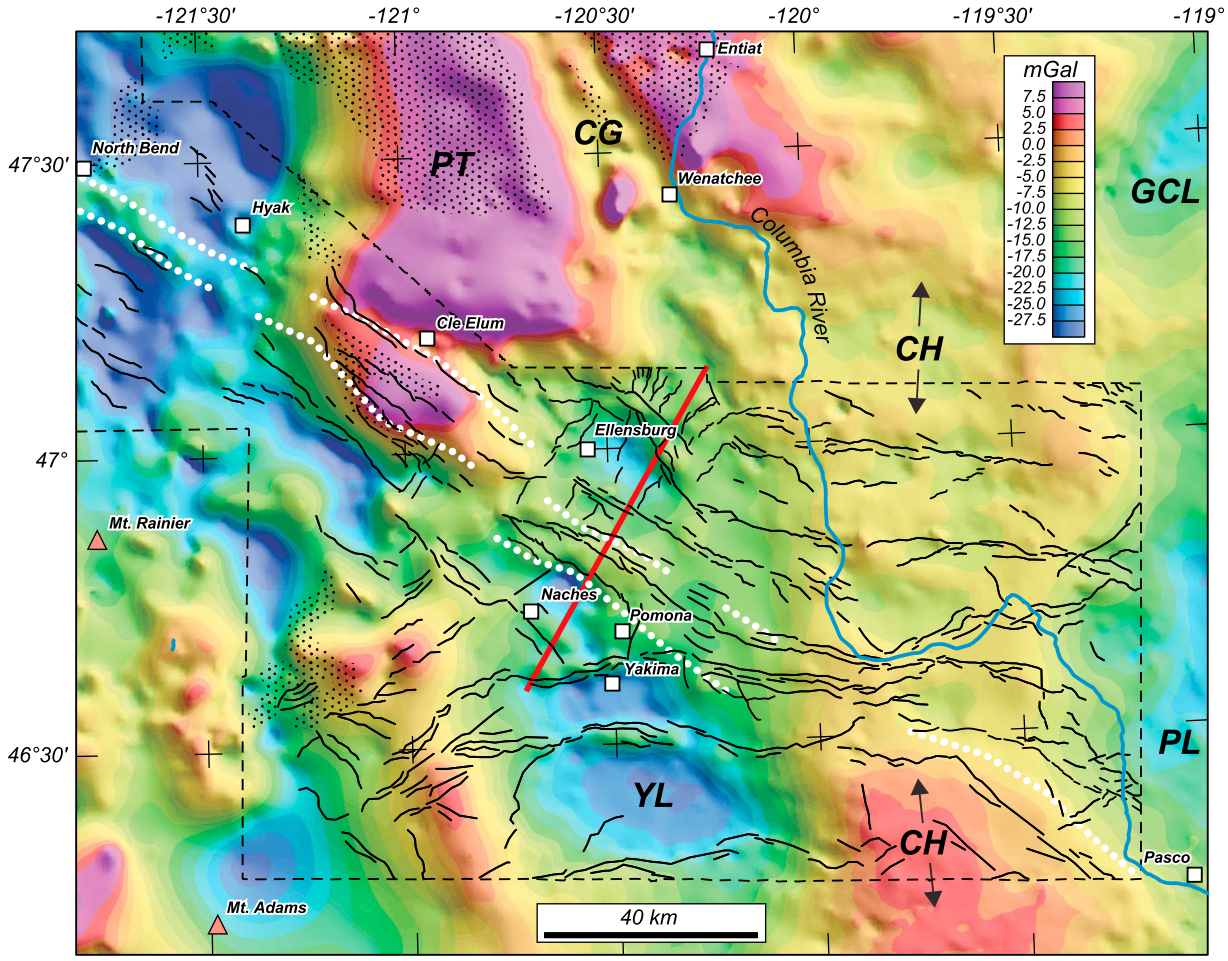

Figure 10. Isostatic residual gravity anomalies of the YFTB and surrounding regions. Stipple pattern indicates exposed pre-Tertiary rocks (Figure 4). Black lines are magnetic lineaments identified in Figure 9. White dotted lines show location of gravity lineament discussed in text. Other labels identify specific anomalies: PT, Pre-Tertiary rocks; YL, Yakima gravity low; PL, Pasco gravity low; GCL, Grand Coulee gravity low; CH, north-south striking central gravity high; CG, Chiwaukum graben. See Figure 6 for description of other items.

1.83 m to 1 m grids) and the U.S. Army Yakima Training Center (1 m grid). Overlaying magnetic anomalies and magnetic lineaments on lidar topography and aerial photography revealed a number of possible fault-related features, including northeast tending fractures and scarps, possible flexural slip scarps along bedding planes, contacts along the flanks of anticlines, and linear scarps. Significant examples are detailed in the following sections.

4.1. Faults and Tectonic Features at Manastash Ridge and Kittitas Valley

[32] Lidar slope images and aerial photography illuminate northeast striking fractures and possible scarps in several places, most notably along Manastash Ridge (western Saddle Mountains) and along the anticlines bordering Kittitas Valley (Figure 9). These features trend dominantly northeastward, do not offset stream drainages, and resemble etched bedrock fractures.

4.1.1. Manastash Ridge Scarp

[33] At least one of these features, on Manastash Ridge, is associated with a topographic scarp, southeast side up, having a maximum height of 2.5 m (Figure 11). This scarp is parallel to and in close proximity to a northeast striking magnetic lineament (Figure 9, label MR), 4.5 km long, with a positive anomaly to the southeast, also suggesting uplift on the southeast side. The magnetic lineament is one of numerous northeast striking anomalies over Manastash Ridge. Other well-expressed northeast trending bedrock features are seen on the northern flank of Manastash Ridge west of the Yakima River and along the northern flank of Manastash Ridge between the Yakima and Columbia Rivers.

4.1.2. Boylston Ridge Scarp

[34] Lidar data also illuminate a northeast trending scarp across the northwestern end of Boylston Ridge in eastern Kittitas Valley, about 16 km east of Ellensburg (Figure 9, label BR; Figure 12). This scarp, here referred to as the Boylston Ridge scarp, trends roughly northeast, is up-thrown on its northwestern side, and is 3–4 m high at its highest point. The scarp crosses a small stream valley adjacent to a highway (streamflow is to the west). Here the stream incises alluvium that fills the valley on the up-thrown side of the scarp, resulting in a narrow ravine (Figure 12). Field

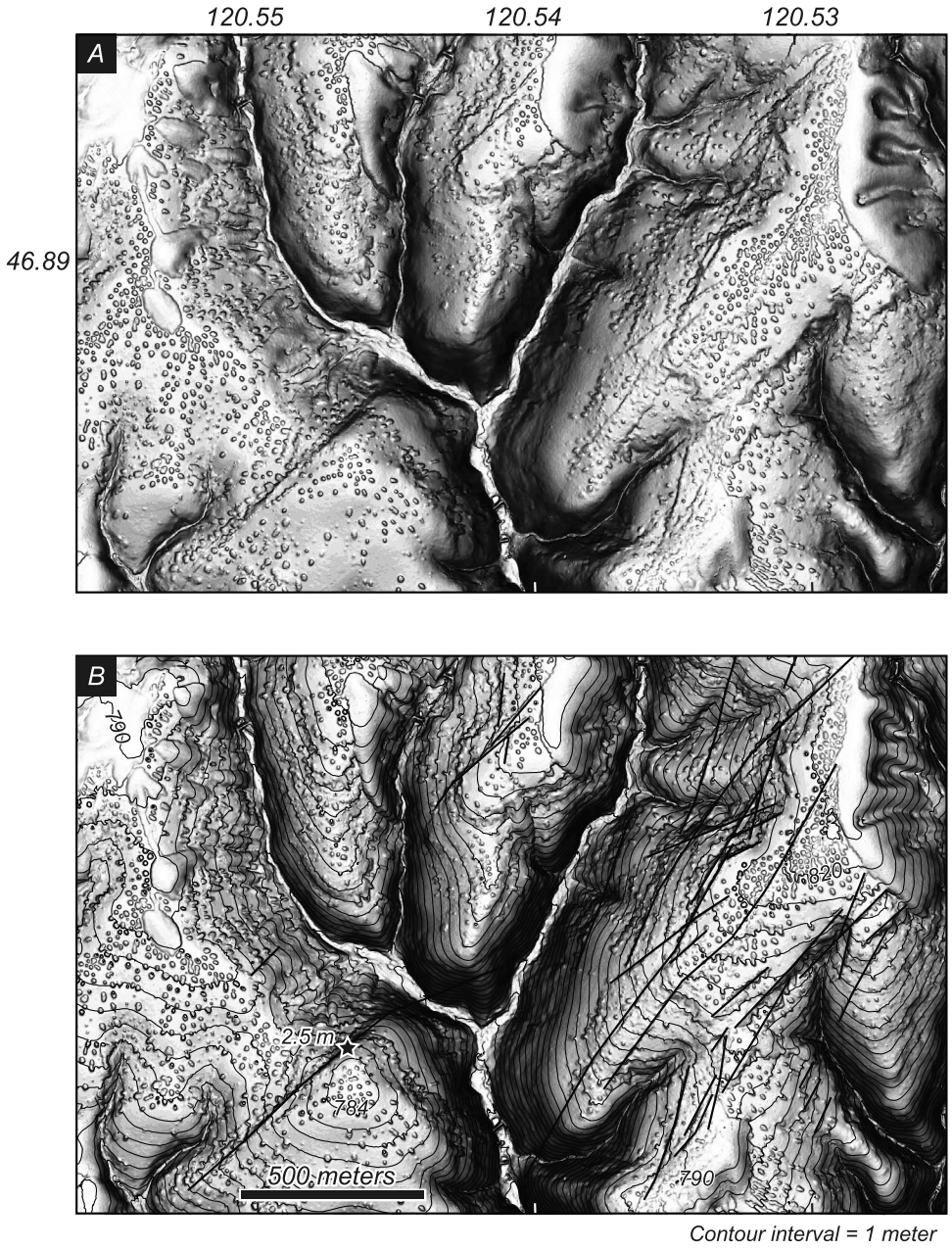

Figure 11. (a) Shaded relief image (azimuth = 315°, altitude = 40°) of a part of Manastash Ridge, overlain by a transparent slope map, generated using a 1 m grid of elevations from airborne lidar survey. (b) Interpreted lidar image showing topographic contours and bedrock fractures (thick black lines). Star indicates the topographic scarp discussed in text.

reconnaissance suggests that a small wetland or pond may have formed in the stream valley at the time the scarp formed. Down-cutting of the stream into late Quaternary alluvium in the valley suggests relatively recent movement. The scarp continues to the northeast and crosses into an alluvium-filled valley (part of Kittitas Valley) and appears to warp the valley surface mapped as Quaternary alluvium.

[35] A complex pattern of magnetic anomalies appears along the Boylston Ridge scarp (Figures 7 and 9, label BR), caused by normally magnetized CRBG exposed at the surface. On close examination, the high-amplitude, short-wavelength magnetic anomalies generally strike north-northwest, oblique to the northeast striking Boylston Ridge scarp. However, magnetic lineaments extending beyond both ends of the Boylston Ridge scarp (Figure 9, label BR) are on strike with the scarp and may help constrain its overall length. A prominent northeast striking anomaly occurs in the Kittitas Valley immediately southwest of Boylston Ridge and lies directly on strike with the scarp. The lineament is positive on its northwestern side, consistent with northwest side up scarp morphology. The broad gradients of this anomaly suggest that its source lies at depth. To the northeast of the Boylston Ridge scarp, a complex pattern of anomalies is similarly on strike with the scarp. Taken together, the lidar

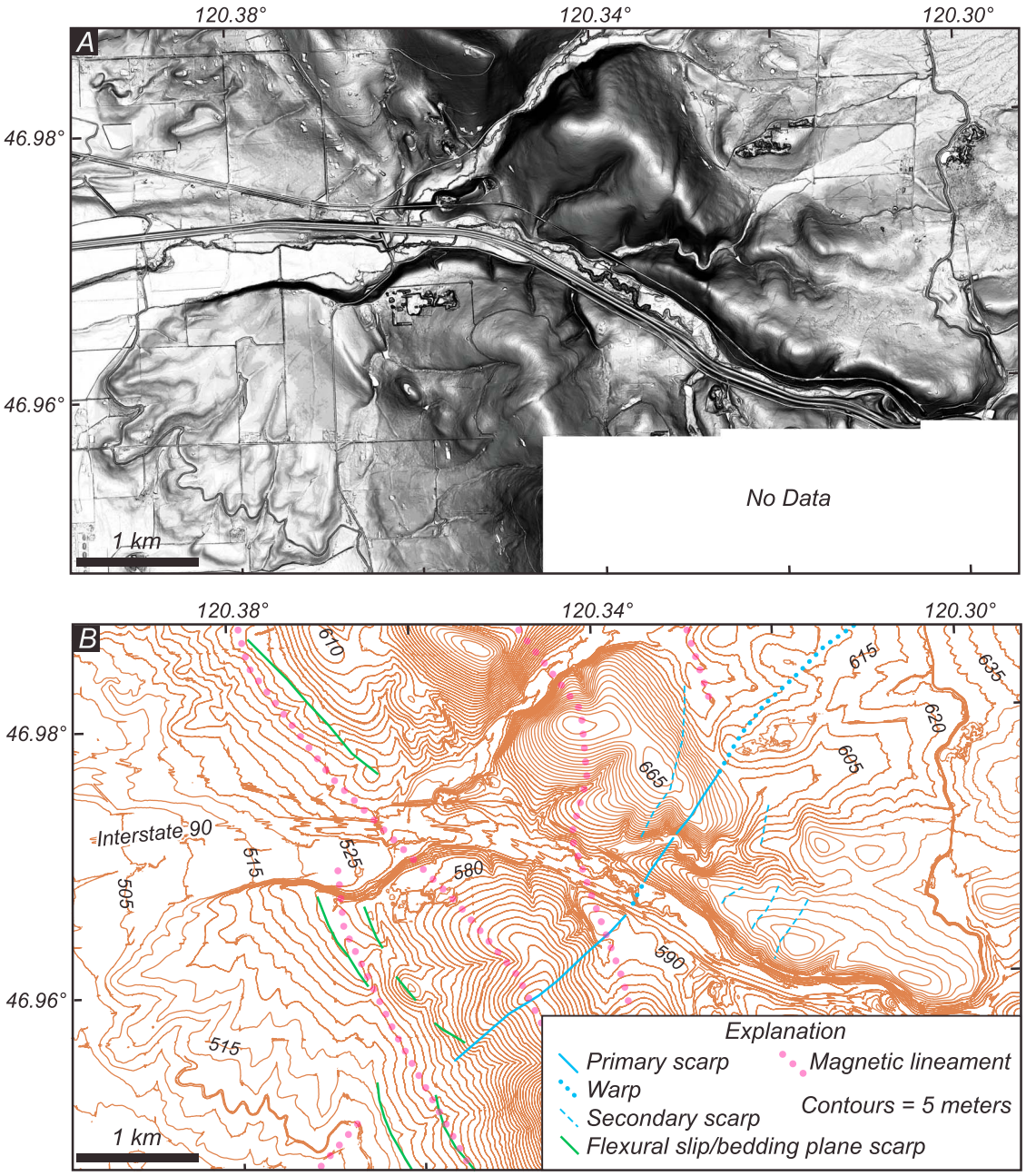

Figure 12. (a) Shaded relief image (azimuth = 315°, altitude = 40°) of Boylston Ridge, overlain by a transparent slope map, generated using a 1 m grid of elevations from airborne lidar survey. Blue line is Boylston Ridge scarp. The small stream in the center of the image flows west. (b) Interpreted lidar image showing topographic contours, magnetic lineaments, possible fault scarp, and bedding plane scarps.

and magnetic data suggest that the Boylston Ridge scarp is a northeast striking fault at least 15 km in length.

4.1.3. Reecer Creek Scarp

[36] *Waitt* [1979] identified a 50 m high, 10 km long scarp in northern Kittitas Valley about 15 km north of Ellensburg, which we refer to here as the Reecer Creek scarp (Figure 9, label RC). The Reecer Creek scarp offsets gravel deposits in the Thorp Formation, a Pliocene fluvial deposit. *Waitt* [1979] noted that the Reecer Creek scarp is associated with both gravity and magnetic anomalies. A ground-based geophysical traverse across the scarp [*Weston Geophysical Research*, 1977; *Waitt*, 1979] found a 500 nT magnetic anomaly and 4 mGal gravity anomaly high immediately south of the scarp. The position of the geophysical anomalies and the south side up topography of the scarp are consistent with a south dipping reverse fault. The age of faulting is constrained by the age of tephra in the youngest part of the Thorp Formation (~3.7 Ma) and undeformed Quaternary fluvial deposits (~130 ka)

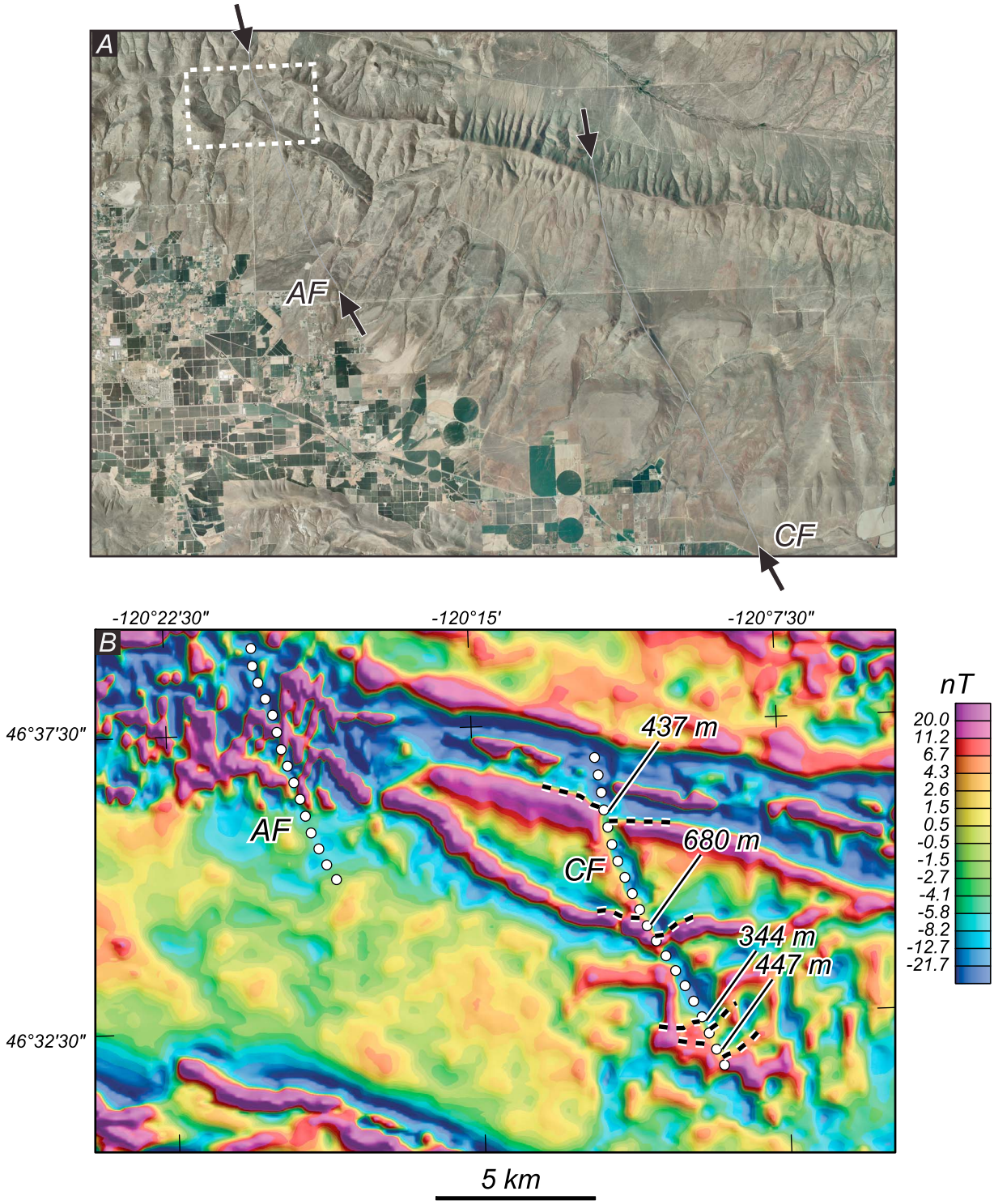

Figure 13. North-northwest striking faults near Yakima, Washington. (a) Aerial photograph of Yakima Ridge. Arrows indicate topographic lineaments. AF, Artesian fault; CF, Coyote Spring fault. White dashed rectangle indicates location of maps on Figure 14. (b) Residual magnetic anomalies of same area. White dotted lines determined from aerial photograph. Pairs of black dashed lines indicate piercing points, with offset indicated by accompanying number.

[*Waitt*, 1979]. The magnetic lineament associated with the Reecer Creek scarp is evident in the new aeromagnetic survey (Figures 7 and 9, label RC), where it can be traced for at least 16 km.

4.2. Right Lateral Faults and Lidar Scarps

[37] Topographic lineaments on aerial photographs reveal two parallel, north-northwest striking faults located 14 and 24 km due east of Yakima, which we here refer to as the

Artesian and Coyote Spring faults (Figures 9 and 13, labels AF and CF), respectively. The strike of both faults is oriented about 60° clockwise from the trend of Yakima Ridge, placing them approximately on strike with the Hog Ranch-Naneum Ridge anticline to the north, a major north trending CRBG structure [*Tolan and Reidel*, 1989; *Schuster*, 1994]. *Schuster* [1994] mapped the Coyote Spring fault with right-lateral displacement. The Artesian fault is not shown by *Schuster* [1994] but is revealed as a scarp/topographic lineament on lidar images. The Artesian fault scarp trends in the same direction as the Coyote Spring fault and displaces ridges in a right-lateral sense, with scarps on opposite sides facing different directions (Figure 14). Ridge crests along the Artesian fault are apparently offset as much as ~150 m in a right lateral manner.

[38] The Coyote Spring fault lies precisely along a sharp, well-defined magnetic lineament (Figure 13b, label CF). Offset magnetic features on opposing sides of the lineament provide at least three pairs of piercing points indicating 300 to 500 m of right-lateral offset on the Coyote Spring fault. The magnetic expression of the Artesian fault is more problematic, but a complex pattern of short-wavelength anomalies does lie subparallel to the scarp (Figure 13b, label AF).

4.3. Umtanum Ridge Bedding Plane Scarps

[39] Bedding-parallel scarps are seen on lidar data along the flanks of several YFTB anticlines. Some of these scarps also lie along prominent magnetic lineaments and mapped faults (Figures 7, 8, and 15). These features may represent flexural slip along bedding planes in the CRBG and intercalated sedimentary units. Some of the more prominent features lie along Umtanum Ridge, Rattlesnake Ridge, and Yakima Ridge west of Hanford. In the following, we illustrate the correlation of these bedding-parallel scarps and magnetic lineaments at Umtanum Ridge, where the ridge is cut by the Yakima River (Figure 15). Similar features lie along the flanks of most anticlines on the Columbia Plateau.

[40] Figure 15 shows a lidar image with interpreted geological features and magnetic lineaments along Umtanum Ridge at the Yakima River canyon. Bedding traces appear on the lidar image in two forms: (1) bedding plane traces that follow topography in flat-lying areas and along dip slopes, and (2) bedding plane scarps that cut across topography in areas of deformed and steeply dipping volcanic and sedimentary rocks. Bedding plane traces tend to lie along gentle dip slopes in broad synclines and follow topographic contours. Bedding plane scarps cut across topographic contours and tend to lie in deformed rocks near the crest of anticlines—in this case Umtanum Ridge—and are roughly parallel to the anticlinal axis and magnetic lineaments associated with the anticline.

[41] The architecture of the Umtanum Ridge anticline is exposed in the Yakima River Canyon at Mount Baldy (Figure 15, label B). Here CRBG dips steeply to the north and corresponds to similar rocks along the northern flank of Umtanum Ridge that produce the bedding plane scarps shown in Figure 15. These bedding plane scarps may represent either differential erosion between adjacent strata or flexural slip scarps along bedding planes within the anticline. Flexural slip scarps have been interpreted as potential seismogenic faults in other fold and thrust belts around the world [*Yeats*, 1986; *Kelsey et al.*, 2008].

[42] A prominent magnetic lineament follows the entire length of the Umtanum Ridge anticline (Figures 2, 6, and 9) and is caused mostly by folded and faulted CRBG of both normal and reversed polarity. One strand of the Umtanum Ridge magnetic lineament passes directly through Mt. Baldy and the Yakima River Canyon (Figure 8). Here the strong magnetic gradient is caused by reversely magnetized R_2 Grande Ronde Basalt exposed in the core of a faulted anticline, overlain by normally magnetized N_2 Grande Ronde Basalt and Wanapum Basalt (Figure 3). The magnetic anomaly at the Yakima River canyon is dominated by these intensely magnetic and deformed rocks, obscuring specific evidence for bedding-parallel faults.

4.4. Umtanum Ridge Fault Scarps

4.4.1. Burbank Scarp

[43] Possible fault scarps lie along the flanks of Umtanum Ridge and separate areas of slope-parallel bedding traces and bedding plane scarps. These scarps also tend to lie near and parallel to magnetic lineaments lying along the flanks of Umtanum Ridge. In particular, a magnetic lineament lies along the mapped trace of a thrust fault—herein referred to as the Burbank fault (Figures 9 and 15, label BF)—that follows Burbank Creek just south and east of Mount Baldy (Figure 15, label B). A scarp identified on lidar images also falls near the magnetic lineament and lies very close to the mapped trace of the Burbank fault [*Schuster*, 1994]. Another scarp, located about 1 km north of Roza Creek, falls directly on a magnetic lineament (Figure 15). The magnetic lineament follows a contact between N_2 Grande Ronde Basalt and the Frenchman Springs Member of the Wanapum Basalt, both normally magnetized. This scarp and its associated magnetic lineament may be the continuation of the Burbank fault on the west side of the Yakima River canyon, where the fault becomes the subsurface contact between Grande Ronde and Wanapum Basalt.

4.4.2. Wenas Scarp

[44] A linear scarp runs along the northern edge of Wenas Valley for about 11 km, approximately 400 m south of the steeply dipping south flank of Umtanum Ridge (Figure 9, label WV; Figure 16). The scarp trends west-northwest and varies in height from ~2 m to over 8 m. The scarp lies on a relatively flat alluvial fan surface, sloping southward toward Wenas Creek at about 1 to 9 degrees. The scarp is parallel to an aeromagnetic lineament that tracks the flank of Umtanum Ridge (Figure 9, label WV). The scarp and magnetic lineament are offset ~400 m, but the scarp follows each bend and wiggle of the magnetic lineament. This close association between scarp and magnetic lineament suggests that the scarp may be structurally controlled and caused by the same structure that generates the magnetic lineament.

[45] Geologic maps and field exposures in the area suggest that the Wenas Valley scarp is related to either recent faulting along the southern flank of Umtanum Ridge or deep-seated landslides (Figure 16). The best way to weigh the merits of these two hypotheses is with trench excavations across the scarp.

4.5. Paleoseismic Trenching

[46] We sited two trenches across the Wenas Valley scarp to observe and map stratigraphy and structure beneath the scarp. One trench was positioned across a ~5 m high seg-

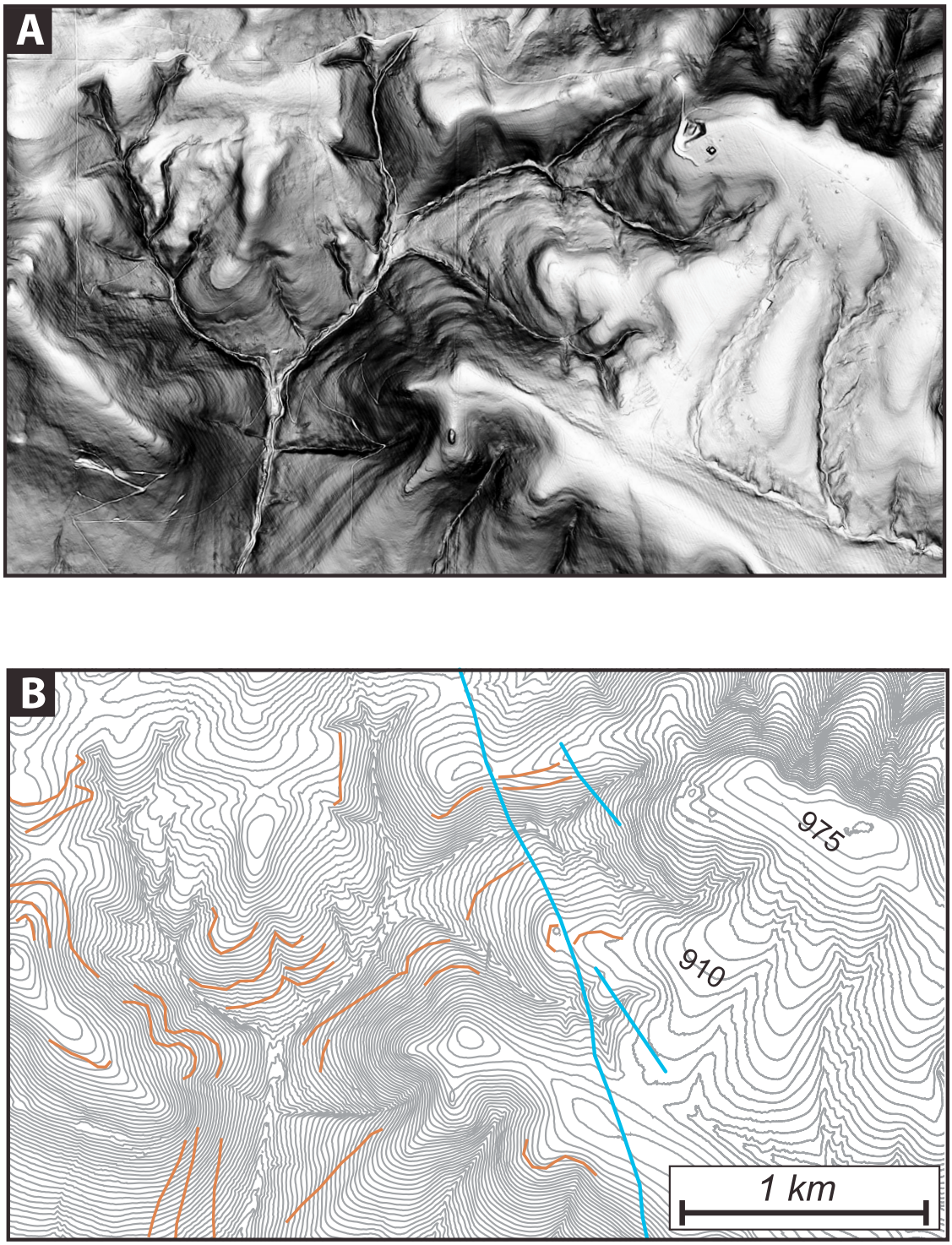

Figure 14. (a) Shaded slope map in the area of the Artesian fault. See Figure 13 for location of map. (b) Topographic contour map showing location of the Artesian fault.

ment of the scarp at Hessler Flat; the second was sited across a ~7 m high segment at McCabe Place. Each excavation was up to 24 m in length and 3 m deep, with walls benched to improve stability. At McCabe Place, we constructed a grid system of 1x1 m cells on one wall of the trench after clearing the wall of loose debris. We marked important stratigraphic and structural contacts with tags of survey tape and nails. Each cell was photographed, and trench logs were constructed by mapping large photomosaics of the cells. At Hessler Flat, we mapped the trench wall directly on scale drawings and transferred field notes to a large photomosaic to create the final trench log.

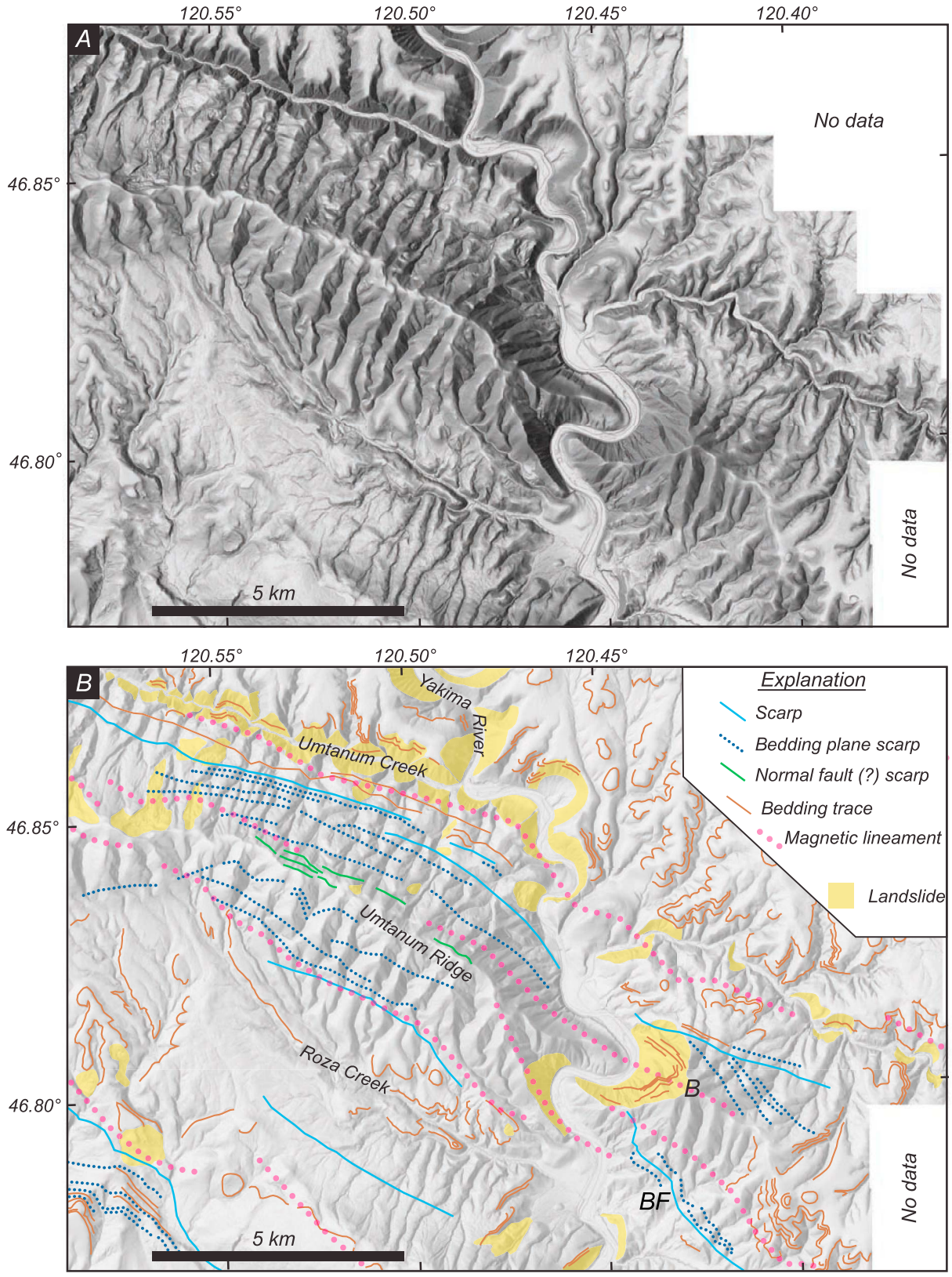

Figure 15. (a) Shaded relief image (azimuth = 315, altitude = 40) of the eastern portion of Umtanum Ridge, overlain by a transparent slope map, generated using a 1 m grid of elevations from airborne lidar survey. (b) Interpreted lidar image showing topographic contours, magnetic lineaments, possible fault scarps, bedding plane scarps, landslides, and bedding plane traces. B, Mt. Baldy; BF, Burbank fault.

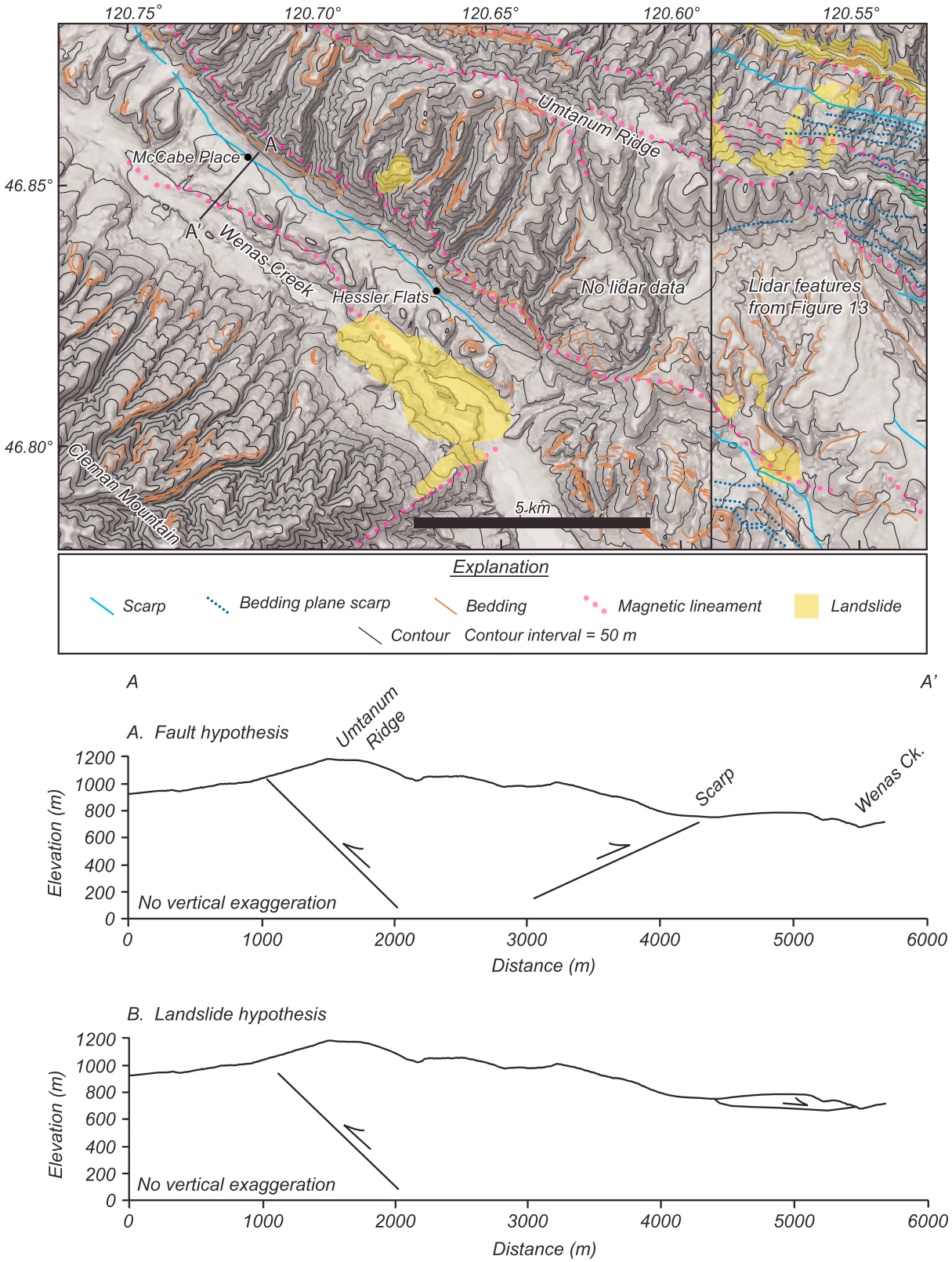

Figure 16. Interpreted shaded slope image of Umtanum Ridge and Wenas Valley, generated using a 10 m DEM. Map shows topographic contours, magnetic lineaments, possible fault scarps, bedding plane scarps, landslides, and bedding plane traces. Black dots are locations of two trench excavations. Cross sections (A-A′) at bottom show two possible interpretations for the Wenas Valley scarp. In cross section B, the Wenas Valley scarp is shown as a landslide headscarp, with the landslide moving along a flat glide plane.

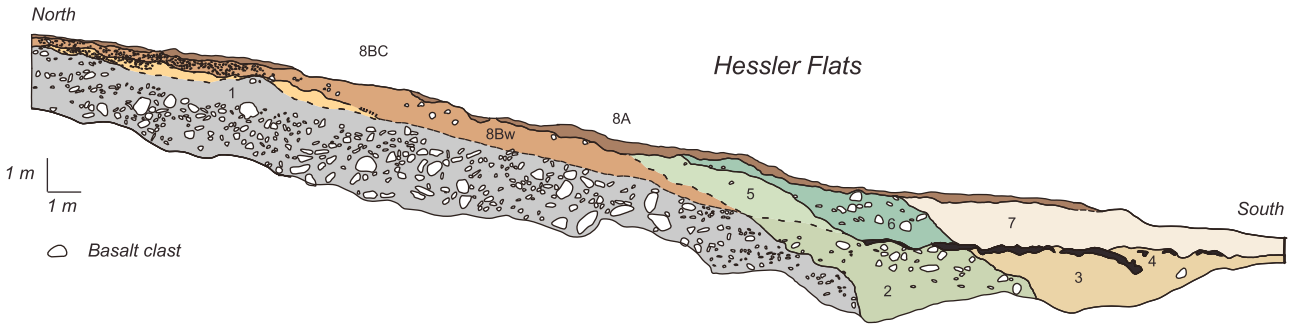

8A	Surface soil A horizon	Dark brown, platy, undisturbed, 10-15cm thick. Contains light gray MSH ash in upper-most part.
8Bw	Colluvium (Bw horizon)	Brown, cobbly, silty, sand between units 1 and 8A. Only appears in hanging wall, or merges with units 4a and 4b. Contact with 4a obscured by trench rubble.
8BC	Colluvium (BC horizon)	Tan, cobbly, silty, sand above unit 1. Only appears on upper tread.
7	Loess	Similar in appearance to unit 5, but contains some cobbles and is slightly less compact. Contains some cobbles, no stratification. Much softer than units 3, 4a, 4b. Slightly lighter and less compact than unit 6.
6	Colluvium	Similar to unit 3, except fewer cobbles, more boulders, a little less dense than unit 4a, darker brown finer grained than unit 3. hard to scrape.
5	Colluvium	Same as unit 3, except few boulders, a little less dense than unit 3, darker brown than unit 3. Very hard to scrape. Contact with unit 8Bw obscured by trench rubble.
4	Buried soil	10-20cm thick, dark brown, silty, few/none cobbles and pebbles. Runs along the top of lower bench. Disappears beneath rubble S of unit 3. Not visible N of unit 6. Possibly disturbed by excavator and/or eroded in places.
3	Loess	Mostly homogenous brown sandy silt appears to onlap unit 3. Contains very few cobbles, no stratification. Much softer than units 3, 4a, 4b. Slightly darker and more compact than unit 6.
2	Colluvium	Brown silty-sandy, semi-consolidated, contains tighly packed cobbles near bedrock. At the contact with unit 3 there is a density change but no color change, and cobbles/boulders disappear. Can be broken into two units, one containing more boulders than the other, which is slightly more cobbly nearest to bedrock.
1	Weathered basalt	Yellowish, highly weathered basalt. Spheroidally weathered into SA boulders and cobbles. Upper contact is at bench and is overlain by a cobbly soil horizon, unit 8BC.

Figure 17. Simplified log of excavation at Hessler Flats.

4.5.1. Stratigraphy

[47] The excavation at Hessler Flat uncovered weathered basalt overlain by alluvium beneath the upper tread above the scarp, and a sequence of loess deposits, a buried soil, and colluvial deposits beneath the lower tread (Figure 17). A sharp down to the south step in the basalt of at least 3.5 m underlies the scarp.

[48] The excavation across the scarp at McCabe Place revealed a sequence of volcaniclastic alluvial deposits, cobble-rich debris flow deposits, angular unconformities, and buried soils (Figure 18). The oldest exposed deposits (units 1 through 3) are white- to cream-colored, sandy silt to cobble-rich silt to sand volcaniclastic deposits. An angular unconformity separates the volcaniclastic deposits from the overlying pumice-rich sandy silt (unit 4). Overlying the sandy silt of unit 4 is a gravelly silty sand (unit 5). Both units 4 and 5 taper out and disappear in the lower third end of the trench. A dark chocolate brown sandy clay (unit 6) displaying well developed prismatic soil structure overlies unit 5 and extends along the entire length of the trench. A sandy silt (unit 7) buries the chocolate brown clay in the lower half of the trench and is missing from the upper part of the trench. Overlying unit 6 in the upper half of the trench is unit 8, a sandy silt similar in lithology to unit 7 but with slightly different color. Unit 8 buries unit 6 in the upper half of the trench but buries unit 7 in the lower half of the trench. The entire sequence is capped by modern surface soil (unit 9), which includes thin pods of tephra from the 1980 eruption of Mount St. Helens.

4.5.2. Faulting/Folding

[49] Relief on the surface of the basalt in the Hessler Flat excavation was possibly caused by folding. The nearest outcrop—a panel of Frenchman Springs Member of the Wanapum Basalt about 300 m away—dips about 22°SSW (Figure 16). Bedding in the Ellensburg Formation is approximately horizontal ~400 m south-southeast of the trench. It is likely, therefore, that basalt at the Hessler Flat trench has a shallow dip (less than 22°SSW and possibly closer to 0°), suggesting that the basalt step observed in the trench is not a reflection of basalt layering and erosion.

[50] We did consider the possibility that valley-wide erosion by Wenas Creek eroded the basalt leaving the scarp at Hessler Flat. We think this is improbable because valley-wide stream erosion would likely remove knobs of Ellensburg Formation, a slightly indurated volcaniclastic deposit, bordering Hessler Flat on the south side. Preservation of these knobs suggests that stream erosion from Wenas Creek was limited to the valley axis. Analysis of digital elevation models shows that Hessler Flat dips gently toward the valley axis, much like modern alluvial fans in the area, whereas modern alluvial surfaces along Wenas Creek slope gently to the east (in a downstream direction). Without exception,

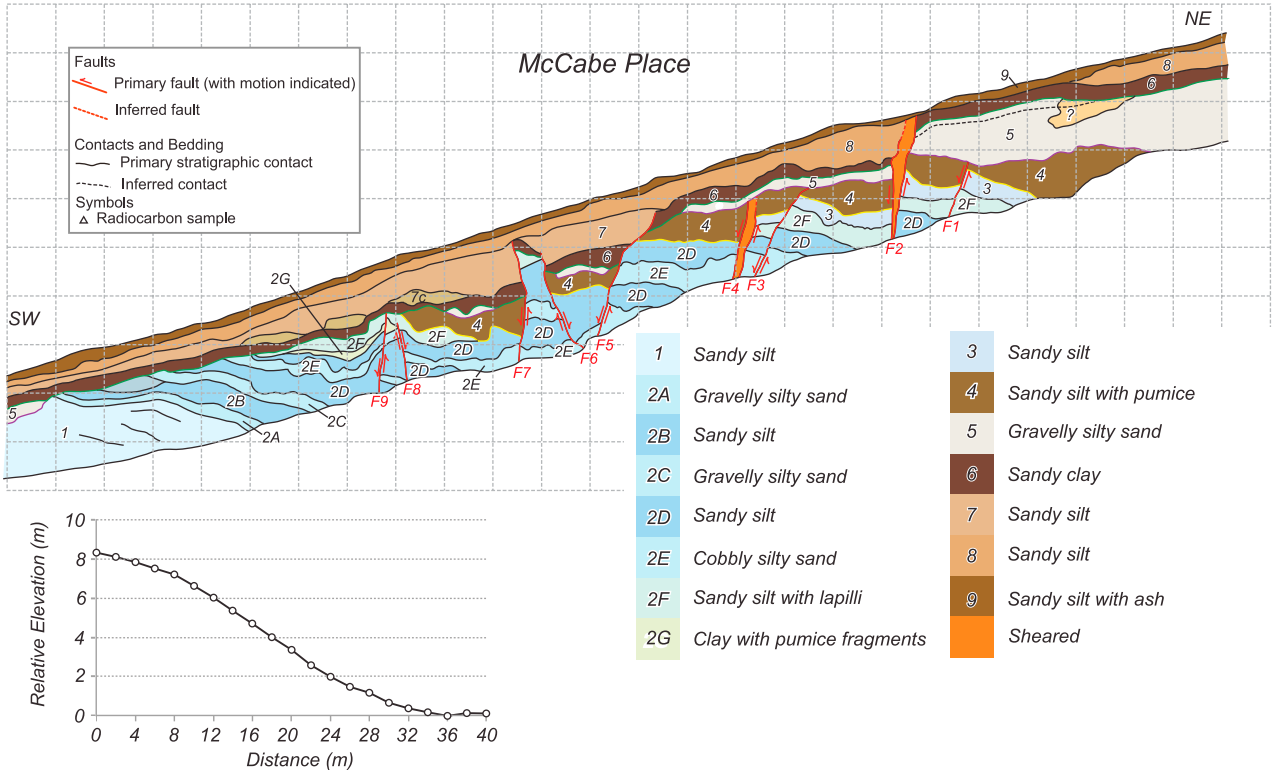

Figure 18. Simplified log of excavation at McCabe Place.

streamflow in the vicinity of Hessler Flat is orthogonal to the scarp, rather than along the scarp. Last, if the scarp is a former fluvial feature, we would expect to find fluvial deposits preserved in the subsurface banked against the scarp, only colluvial deposits and loess banked against the scarp were observed.

[51] The stratigraphic sequence exposed in the McCabe excavation is broken by several normal faults (Figure 18, labels F1 to F9). The oldest units also show evidence for folding (Figure 18). Bedding in units 1 to 3 and the unconformity between units 3 and 4 form a slight arch, with the apex of the arch about in the center of the excavation. F1 to F5 are normal faults that offset the stratigraphy in a down to the south fashion. F6 to F9 are normal faults that bound two horsts, with the southernmost horst bounded on the down-thrown side by a small syncline.

[52] The stratigraphy, unconformities, and faults exposed in the McCabe excavation suggest at least three episodes of deformation. The total amount of normal faulting is ~3 m, while the total scarp height is ~7 m, suggesting substantial deformation not accounted for by faults evident in the trench. Bedding in the volcaniclastic alluvium is folded and could account for the discrepancy between scarp height and observed faulting. The small syncline adjacent to one of the horsts suggests that contraction accompanied movement on F8 and F9, which predated movement on the other horst bounded by F7 and F6. The most recent episode of movement is on fault F2, which extends through the entire stratigraphic package except for the modern soil, suggesting a relatively recent age for movement along this fault.

[53] We favor an interpretation that the possible folding/faulting of basalt at Hessler Flat and normal faulting at McCabe Place are due to bending moment normal faulting in the hanging wall of an oblique and blind thrust fault. The blind thrust may be the cause of the aeromagnetic lineament 400 m to the north that closely parallels the entire Wenas Valley scarp. Although alternative explanations for the Wenas Valley scarp are possible, such as the headscarp of a shallow landslide or erosion along bedding planes, the length and morphology of the scarp favors a fault origin.

4.6. Wooded Island Earthquake Swarm

[54] A swarm of over 1000 microearthquakes occurred from January through June 2009 in the vicinity of Wooded Island in the Columbia River about 8 km north of Richland, Washington (Figure 9, label WI; Figure 19). Hypocenters were concentrated in an area about 2 km^2 and less than 2 km deep. The largest earthquake was M_W 3.0, with recorded peak ground accelerations of 0.15 g in the horizontal direction and 0.02 g in the vertical direction [*Rohay*, 2009]. The first motions of the largest earthquake were consistent with a northwest striking reverse fault [*Thelen et al.*, 2009] (see also Pacific Northwest Seismic Network, http://www.pnsn.org/welcome.html, 2010). The earthquake swarm was accompanied by about 35 mm of surface deformation observable in satellite interferometry [*Wicks et al.*, 2009]. Models of this deformation are consistent with 50 mm of slip on a west-northwest striking reverse fault and associated bedding plane fault in underlying CRBG [*Wicks et al.*, 2009].

[55] The Wooded Island earthquake swarm occurred about 16 km northeast of the Rattlesnake Mountain fault (Figures 2 and 19, label RM) and about 17 km south of the Gable Mountain fault (Figures 2 and 19, label GM). Both of these YFTB structures produce distinct magnetic anomalies

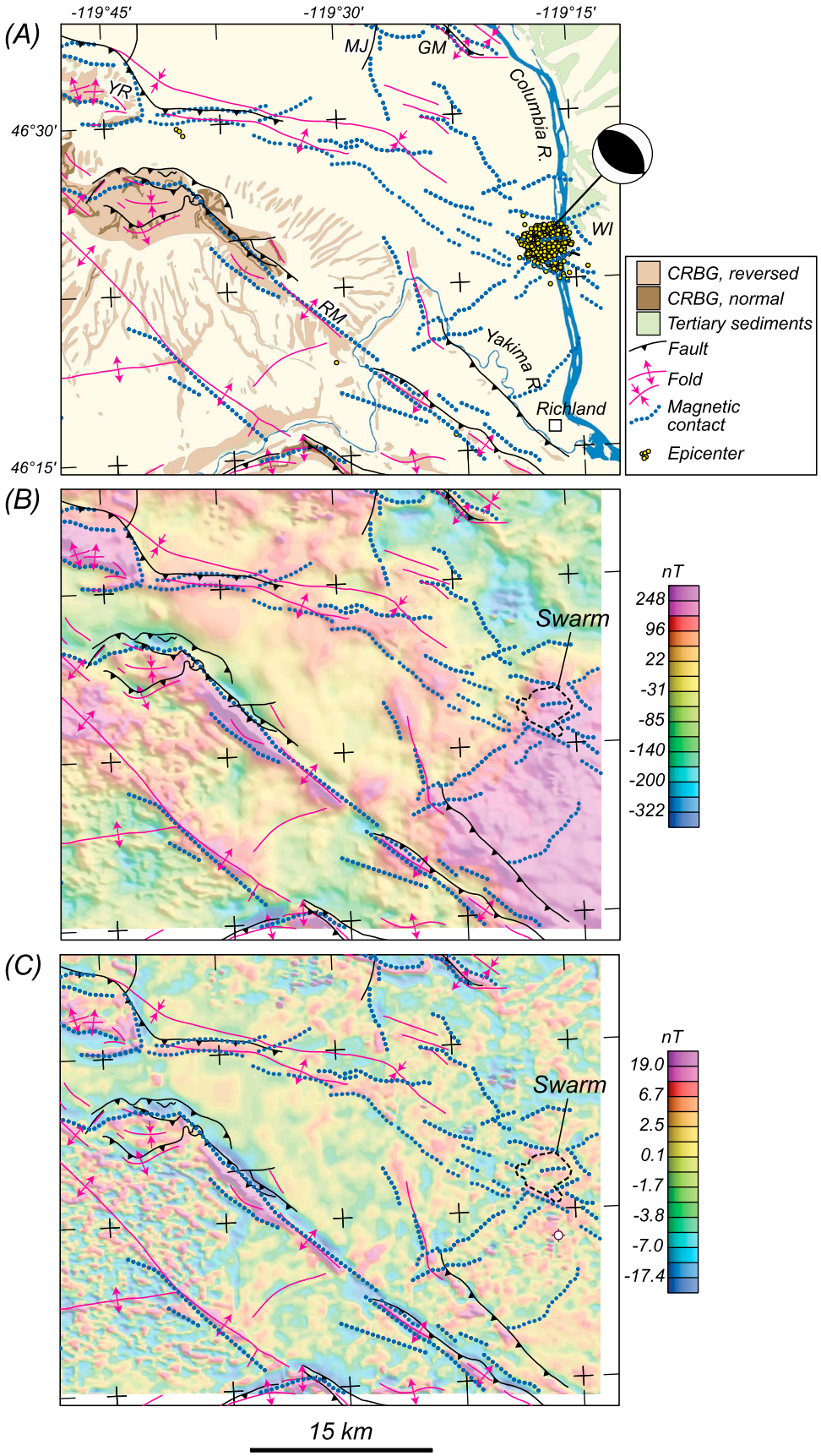
(A)
-119°45'
-119°30'
-119°15'
46°30'
46°15'
MJ
GM
YR
Columbia R.
WI
RM
Yakima R.
Richland
CRBG, reversed
CRBG, normal
Tertiary sediments
Fault
Fold
Magnetic contact
Epicenter
(B)
Swarm
nT
248
96
22
-31
-85
-140
-200
-322
(C)
Swarm
nT
19.0
6.7
2.5
0.1
-1.7
-3.8
-7.0
-17.4
15 km

Figure 19

(Figures 6–8), but other more subtle lineaments in the immediate vicinity of Wooded Island may be relevant to the earthquake swarm itself. Without exception, positive magnetic anomalies overlie mapped anticlines in this area (Figure 19). Notable examples include linear magnetic anomalies over Yakima Ridge and Rattlesnake Mountain. While the correlation between magnetic anomalies and anticlines is not surprising, it does present an interesting puzzle: Most exposures of CRBG in this area are magnetized in reversed directions (Figure 19a), which would predict negative magnetic anomalies over anticlines. The presence of positive anomalies suggest that the exposed, reversely magnetized CRBG sections may be thin relative to underlying normally magnetized units. This interpretation is supported to some extent by geologic mapping [*Reidel et al.*, 1989a], which shows that reversely magnetized flows exposed in this area are 30 to 50 m thick, while underlying normally magnetized Wanapum Basalt (Figure 3) is >180 m thick. However, an even thicker section of reversely magnetized Grande Ronde R_2 underlies the Wanapum Basalt, adding complexity to the puzzle.

[56] Linear anomalies over Yakima Ridge and Rattlesnake Mountain extend southeastward beyond exposed CRBG, suggesting that the structures causing the anomalies also extend southeastward in the subsurface. This interpretation is consistent with the depth to the top of CRBG as determined from closely spaced boreholes in this area [*Thorne et al.*, 2006]. For example, borehole depth to CRBG defines a subsurface ridge extending southeastward from Yakima Ridge, coincident with the magnetic anomaly, to about longitude 119°26′W. The CRBG ridge seen in borehole data does not obviously continue east of this longitude, however, where the linear anomaly has low amplitude (~100 nT). A simple forward model of the Yakima Ridge magnetic anomaly near Wooded Island shows that the anomaly could be caused by a small (<100 m) anticlinal fold on the top of basalt. Unfortunately, the distribution of boreholes would not have resolved this small fold at this location.

[57] The magnetic anomaly here interpreted to be caused by the Yakima Ridge anticline continues discontinuously to the Columbia River and beyond, where the source of the anomaly is entirely concealed by Quaternary sediments. Along this reach we see subtle hints of uplift in 7.5 min topographic maps and in a discontinuous pattern of late Pleistocene Missoula flood deposits exposed through younger dune sands. Lineaments associated with this anomaly pass immediately south of the Wooded Island earthquake swarm, where they strike parallel to subtle patterns in the distribution of epicenters. We presume that the entire anomaly, including the segment south of Wooded Island, is caused by a continuation of Yakima Ridge beneath the Hanford reservation. Near Wooded Island, the ridge is now completely eroded by successive Pleistocene floods and buried beneath younger fluvial sediments.

[58] A second magnetic lineament strikes northeastward, orthogonal to the Yakima Ridge anomaly and directly through the Wooded Island earthquake swarm. This broad gradient is evident in the original magnetic anomalies (Figure 19b) but barely discernible in anomalies filtered to emphasize shallow sources (Figure 19c), suggesting that its source lies at significant depth, probably deeper than borehole penetration in this area. The sense of the anomaly, with more positive values to the east, is consistent with an up to the east fault. Its northeast strike is parallel to nearby faults, notably the May Junction fault located 20 km to the north, which cuts Pleistocene Hanford Formation (Figure 19a, label MJ) [*Repasky et al.*, 2009]. Other interpretations are possible, of course. For example, the anomaly could indicate the northwestern extent of the Ice Harbor Member (Figure 3), a relatively young and normally magnetized CRBG unit.

[59] *Wicks et al.* [2009] have shown that surface deformation associated with the Wooded Island earthquake swarm is consistent with displacement on two faults: a northwest striking, northeast dipping reverse fault and an adjacent bedding pane fault immediately to the northeast. The reverse fault lies within CRBG of our hypothesized southeastward continuation of the Yakima Ridge anticline, and the bedding plane fault lies within the northeast limb of the same anticline. The dip of the bedding plane fault could be as much as 30° [*Wicks et al.*, 2009], consistent with the limb of this small anticline. We suggest that the Wooded Island earthquake swarm was caused by slip on both the reverse and bedding plane faults in response to horizontal compression across the concealed Yakima Ridge anticline.

5. Discussion

[60] Folded and faulted stratigraphy of the CRBG produces distinctive magnetic anomalies, including dramatic lineaments along each of the major YFTB anticlines (Figures 6–8). Quaternary faults are mapped along most of the YFTB anticlines (http://earthquake.usgs.gov/hazards/qfaults), and we should consider the possibility that magnetic lineaments elsewhere in the YFTB reflect unmapped Quaternary faults. In this study, we are especially interested in the Frenchman Hills, Saddle Mountains, and Umtanum Ridge anticlines and associated Quaternary faults (Figure 2) because, west of the Columbia River, these structures strike northwestward toward active faults in the Puget Lowland. In this regard, the Umtanum Ridge anticline is likely the most significant: Magnetic lineaments associated with the Frenchman Hills and Saddle Mountains faults merge with north-northwest trending anomalies along the east side of Kittitas Valley east of Ellensburg (Figure 9), suggesting that the Frenchman Hills

Figure 19. (a) Geologic map of the Wooded Island area, generalized from *Schuster et al.* [1997]. Yellow symbols show all earthquakes with $M_W \geq 1$ occurring from January 1, 2009, to April 23, 2010. Focal mechanism is for largest earthquake (M_W 3.0), which occurred on May 4, 2009 (Pacific Northwest Seismic Network, http://www.pnsn.org/welcome.html, 2010). Blue dotted lines are magnetic contacts interpreted from aeromagnetic anomalies. MJ, May Junction fault; GM, Gable Mountain fault and anticline; YR, Yakima Ridge; RM, Rattlesnake Mountains anticline; WI, Wooded Island. (b) Unfiltered magnetic anomalies, with interpreted magnetic contacts and mapped structures. Black dashed line outlines Wooded Island earthquake swarm. (c) Magnetic anomalies filtered in order to emphasize shallow magnetic sources.

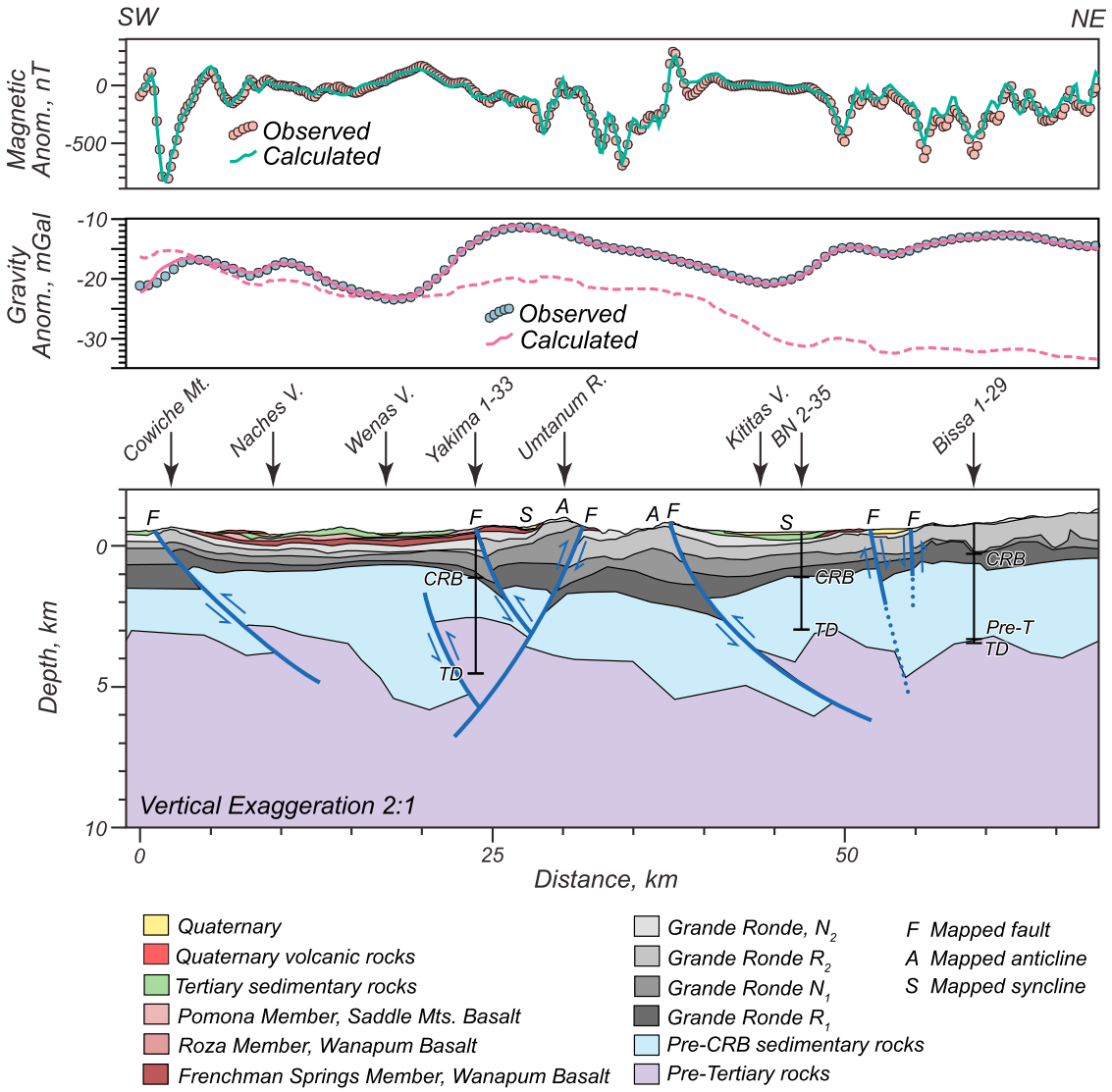

Figure 20. Crustal model across Umtanum ridge. Forward model is based on gravity and magnetic data constrained by geologic mapping and three deep exploratory boreholes. Model assumed infinitely extended in the directions perpendicular to the profile. Dashed gravity profile is calculated anomaly without pre-Tertiary interface. See Figures 4, 6, and 10 for profile location. See Table 1 for magnetizations and densities used. Well labels: CRB, base of CRBG; Pre-T, top of pre-Tertiary; TD, total depth of penetration.

and Saddle Mountains faults do not serve as throughgoing structures to the Puget Lowland. On the other hand, magnetic lineaments of the Umtanum Ridge anticline continue west-northwestward well into the Cascade Range.

[61] Figure 10 shows that the Umtanum Ridge fault is spatially associated with a positive gravity anomaly extending from longitude 120°W to at least longitude 121°45′W. This gravity anomaly overlies pre-Tertiary basement south of Cle Elum, and we postulate that the entire positive anomaly is caused by shallow basement rocks extending from the YFTB into the Cascade Range. The correlation between Umtanum Ridge magnetic lineaments and the basement gravity high has several important implications: First, it further supports a connection between Quaternary deformation in the YFTB and Puget Lowland. Second, faults associated with this Quaternary deformation may extend through the sub-CRBG Tertiary section and into pre-Tertiary basement rather than shoaling into CRBG stratigraphy.

5.1. Umtanum Ridge Gravity and Magnetic Model

[62] Figure 20 shows a cross section through Umtanum Ridge calculated from gravity (Figure 10, red line) and magnetic (Figure 6, red line) anomalies and constrained by geologic mapping [*Walsh et al.*, 1987; *Dragovich et al.*, 2002] and three deep boreholes drilled for hydrocarbon exploration [*Reidel et al.*, 1989b]. Table 1 provides the rock magnetic and density properties used in the model. We have assumed in this model that magnetic anomalies are caused primarily by highly magnetic CRBG, with both normal and reversed polarities, whereas gravity anomalies are caused

Table 1. Physical Properties Used in Umtanum Ridge Gravity and Magnetic Model[a]

	$\Delta\rho$	χ	M_R
Quaternary sediments	−250	0	0
Quaternary volcanic rocks	−200	0	1.06 R
Tertiary sedimentary rocks	−200	0	0
Pomona Member, Saddle Mts. Basalt	0	6.28	2.5 R
Roza Member, Wanapum Basalt	0	6.28	2.5 R
Frenchman Springs Member, Wanapum Basalt	0	3.95–11.57	2.5 N
Grande Ronde, N_2	0	6.28	2.5 N
Grande Ronde, R_2	0	6.28	4.0 R
Grande Ronde, N_1	50	6.28	2.5 N
Grande Ronde, R_1	100–120	6.28	2.5 R
Sub-CRBG sedimentary rocks	−100	0	0
Pre-Tertiary rocks	200	0	0

[a]See Figure 20. $\Delta\rho$ = density contrast relative to Bouguer reduction density (2670), kg/m^3; χ = magnetic susceptibility in SI units, multiplied by 1000; M_R = remanent magnetization, A/m (N normal, R reversed).

mostly by topography on underlying pre-Tertiary basement [*Saltus*, 1993]. Remanent magnetization directions were assumed parallel or antiparallel to the field of a geocentric dipole.

[63] Our model honors deep borehole information except in one location. Our model shows borehole Yakima 1–33 penetrating well into pre-Tertiary rocks, even though pre-Tertiary rocks were not encountered in this hole (Figure 20). We feel that the pronounced positive gravity anomaly in this location demands a shallowing of the pre-Tertiary interface. The discrepancy between our model and borehole stratigraphy probably reflects the fact that the borehole is 9 km distant from the profile in a region where gravity anomalies vary in the direction normal to the profile.

[64] Densities and magnetizations of CRBG units are critical to our model. In his three-dimensional inversion, *Saltus* [1993] inferred densities from four borehole gravity studies, three at the Hanford site and one in the Rattlesnake Hills [*Robbins et al.*, 1979]. These measured densities range from 1600 to 2900 kg/m^3, depending on the relative amounts of competent basalt, fractured basalt, rubble, and volcaniclastic rocks. We follow *Saltus* [1993] and assume that deep CRBG units have higher densities than shallow CRBG units. Our densities are somewhat higher than those used by *Saltus* [1993] to reflect high density values observed in a fifth borehole gravity study [*MacQueen and Mann*, 2007] not available to Saltus at the time.

[65] Umtanum Ridge is modeled in Figure 20 as a transpressive uplift bounded on its northeast and southwest sides by opposing thrust faults. In this view, the thrust along the northeast margin of Umtanum Ridge is the primary structure. Note that faults are modeled in Figure 20 as penetrating through the entire CRBG section and into underlying pre-Tertiary rocks. Admittedly, this latter interpretation is not well constrained by gravity and magnetic modeling; however, gravity anomalies do require the presence of significant topography on high-density basement rocks at this location. As shown by the dashed profile in Figure 20, it is not possible to fit observed gravity anomalies with a geologically reasonable cross section unless offsets of deeply buried, high-density basement rocks are included.

5.2. Connecting the Yakima Fold and Thrust Belt to Puget Lowland Structures

[66] As described in the preceding sections, abundant evidence exists for Quaternary deformation both east and west of the Washington Cascade Range, and recent geologic mapping [e.g., *Dragovich et al.*, 2009a, 2009b] has described Quaternary faulting in parts of the Cascade Range itself. Exposed Tertiary plutons in the Cascade Range imply long-term uplift and compressional tectonism. Exhumed granitic plutons as young as 14 Ma [*Mattinson*, 1977] within the Cascade Range and the relatively high elevations and eastward regional tilt of CRBG on the east side of the Range [e.g., *Mitchell and Montgomery*, 2006] testify to Miocene and younger uplift. (U-Th)/He ratios and fission track data further indicate a pulse of rapid Cascade Range uplift (0.5–1.5 km/m.y.) since 12 Ma, and high exhumation rates may persist locally today [*Reiners et al.*, 2002].

[67] A series of parallel structural and magnetic lineaments imply the continuation of the YFTB through the Cascade Range (Figure 21). These structural/magnetic zones include the White River-Naches River fault zone (Figure 21, label WRF and NRF), the Mount Lindsay structural zone (Figure 21, label ML), and the Green River structural zone (Figure 21, label GR).

5.2.1. White River-Naches River Fault Zone

[68] The White River-Naches River fault zone, the southernmost of the structural zones, is perhaps the best example of a link between the YFTB and active Puget Lowland faults. This fault zone consists of several en echelon faults and folds that together extend entirely across the Cascade Range, from Enumclaw to Naches, Washington. On the west side of the Cascade crest, the fault zone follows the White River drainage (Figure 21, label WRF), where it separates Oligocene Ohanapecosh Formation to the north from Miocene Fifes Peak Formation to the south [*Tabor et al.*, 2000]. On the east side of the Cascade crest, it follows the Naches River drainage (Figure 21, label NRF) from the Cascade crest to the base of Cleman Mountain (Figure 21, label CM), where it merges with the Umtanum Ridge fault zone [*Tolan and Reidel*, 1989]. From the Cascade crest to Naches Pass, the White River-Naches River fault zone separates Oligocene Ohanapecosh Formation to the north from Miocene Fifes Peak Formation. Farther east, the zone juxtaposes Eocene-Oligocene Naches Formation to the north against Ohanapecosh Formation and Miocene Grande Ronde Basalt (CRBG) to the south [*Schuster et al.*, 1997].

[69] Elements of the White River-Naches River fault zone produce distinct magnetic anomalies. Most anomalies lie near and parallel to mapped fault segments or fold axes within the zone (Figure 21b). Taken together, the mapped faults, folds, and magnetic lineaments comprise a fault zone that extends at least 100 km from Enumclaw to Naches. On the basis of magnetic anomalies, we argue that the White River-Naches River fault zone merges with the Umtanum Ridge fault northeast of Cleman Mountain, as described by *Tolan and Reidel* [1989]. The fault zone may be significantly longer still, depending on how and if it traverses the Puget Lowland. Weak gravity anomalies [*Danes and Phillips*, 1983] and magnetic lineaments in the eastern Puget Lowland may indicate the continuation of the White River-Naches River

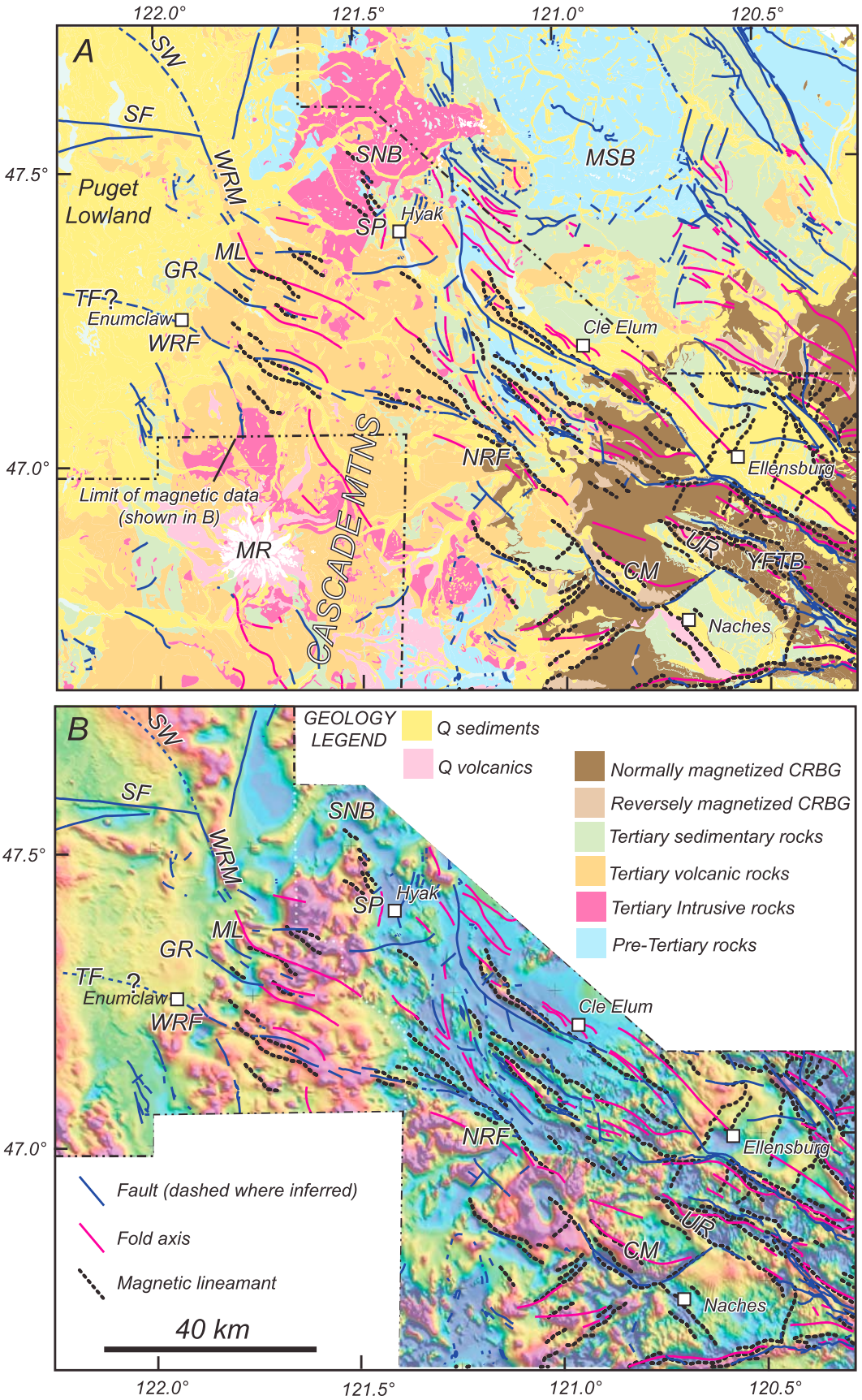
A
B
122.0°
121.5°
121.0°
120.5°
47.5°
47.0°
SW
SF
WRM
Puget
Lowland
SNB
MSB
SP
Hyak
ML
GR
TF?
Enumclaw
WRF
Cle Elum
CASCADE MTNS
NRF
Ellensburg
Limit of magnetic data
(shown in B)
MR
UR
CM
Y.F.T.B.
Naches
GEOLOGY
LEGEND
Q sediments
Q volcanics
Normally magnetized CRBG
Reversely magnetized CRBG
Tertiary sedimentary rocks
Tertiary volcanic rocks
Tertiary Intrusive rocks
Pre-Tertiary rocks
Fault (dashed where inferred)
Fold axis
Magnetic lineamant
40 km

Figure 21

fault zone merging with the Tacoma fault in the western Puget Lowland (Figure 21, label TF). If so, the White River-Naches River fault zone extends from near the Olympic Mountains to Umtanum Ridge, a distance greater than 185 km.

5.2.2. Mount Lindsay and Green River Structural Zones

[70] The northern limit of YFTB deformation in the Cascade Range is marked by a northwest striking lineament that we informally call the Mount Lindsay structural zone (Figure 21, label ML). Mount Lindsay itself is a syncline, with Miocene Fifes Peak Formation in its core and Miocene-Oligocene Eagle Gorge volcanic rocks and Oligocene Ohanapecosh Formation on the limbs. A prominent magnetic anomaly follows the trend of the synclinal axis. The northwest ends of the Mt. Lindsay syncline and its magnetic anomaly swing northward toward the north striking western Rattlesnake Mountain fault (Figure 21, label WRM) zone in the foothills of the Cascade Range [*Dragovich et al.*, 2009a, 2009b]. (We add the adjective "western" in order to distinguish this Rattlesnake Mountain fault in the western Cascades from the better known Rattlesnake Mountain fault in the YFTB.) Evidence for Quaternary faults in the Cascade Range is generally sparse, but the western Rattlesnake Mountain fault zone is an exception, where *Dragovich et al.* [2009a, 2009b] have mapped numerous north striking normal faults. Volcanic rocks associated with the western Rattlesnake Mountain fault zone produce a linear, high-amplitude magnetic anomaly directly over western Rattlesnake Mountain (Figure 21b).

[71] We suggest that the northwest striking Mount Lindsay fold (Figure 21, label ML) provides the mapped location of a possible link between the Quaternary Umtanum Ridge fault and the southern end of the western Rattlesnake Mountain fault zone (Figure 21, label WRM). The anomaly over western Rattlesnake Mountain continues northward beyond the mapped extent of the fault zone, where it connects with the southwestern end of the active Southern Whidbey Island fault (Figure 21, label SW). In this interpretation, the Umtanum Ridge and Southern Whidbey Island faults are segments of a throughgoing structure extending from eastern Washington to the Olympic Peninsula, with a right step along the western Rattlesnake Mountain fault zone. In this view, the active Seattle fault is a westward splay from the main throughgoing structure (Figure 21), as also suggested by *Dragovich et al.* [2009b]. We consider the throughgoing structure to be the northwestern portion of the OWL.

[72] The Green River structural zone (Figure 21, label GR) lies midway between the White River fault zone and the Mount Lindsay structural line. This zone consists of a down to the south reverse fault that places Eocene Puget Group sedimentary and volcanic rocks against Oligocene Ohanapecosh Formation. The fault follows the Green River eastward into the Cascade Mountains, where the fault parallels a syncline and an anticline mapped in Tertiary sedimentary and volcanic rocks. If continued eastward, these features would merge with structures in the Yakima fold and thrust belt.

5.3. Earthquake Hazard Assessments

[73] Figure 22 summarizes the foregoing discussion linking major fault systems of northwestern Washington through the Cascade Range to the YFTB. In the Puget Lowland, the Southern Whidbey Island, Tacoma, and Seattle faults produced multiple $M_w > 6.5$ earthquakes in Holocene time, and the general distribution of crustal earthquakes during the past few decades (Figures 2 and 22) suggests that Puget Lowland faults are active today.

[74] A possible link between these active Puget Lowland faults and the YFTB may warrant a reexamination of the treatment of earthquake hazards in eastern Washington. Since 1996, USGS National Seismic Hazards Maps [*Frankel et al.*, 1996] have treated earthquake hazard assessments in western Washington differently from assessments in eastern Washington. First, from the Cascade Range eastward, background seismicity zones have taken into account tectonic provinces with low historical seismicity but still capable of producing large magnitude earthquakes. The background seismicity zone for eastern Washington is part of a much larger zone that includes most of the Basin and Range in the western United States and portions of stable North America (e.g., Idaho batholith, Okanogan Highlands, Blue Mountains). Second, since 2002 [*Frankel et al.*, 2002], Puget Sound hazard calculations have included an areal zone of hazard, in addition to well-documented faults (e.g., the Seattle and Southern Whidbey Island faults), in an effort to account for undiscovered crustal faults. Third, because so little fieldwork has been conducted on faults in eastern Washington since the mid-1990s, crustal faulting parameters for the YFTB used in the 2008 National Seismic Hazard maps are essentially the same as those used in the 1996 version [*Petersen et al.*, 2008].

[75] Our model suggests that the YFTB portion of eastern Washington tectonically links to Puget Sound through the Cascade Range. The linkage in our model is similar to the block tectonic model of *McCaffrey et al.* [2007], where differences in measured crustal slip distribution between eastern and northwestern Washington require similar linkage through the Cascades. Our trenching in Wenas Valley on the Umtanum Ridge system has identified previously unknown late Quaternary/Holocene earthquakes and/or tectonic deformation episodes. Lidar data and aeromagnetic interpretations identified several other potential faults where future trenching is likely to confirm late Quaternary or Holocene faulting. Thus, the developing understanding of the YFTB, where major faults have both characteristic aeromagnetic and lidar signatures, is remarkably similar to results already found for faults in Puget Sound. Further, as noted above, the YFTB has significant crustal seismicity loosely related to mapped faults (Figure 22b), similar to

Figure 21. Possible structures linking Quaternary faults of the Yankima fold and active faults of the Puget Lowland. (a) Geologic map generalized from *Schuster et al.* [1997], *Walsh et al.* [1987], *Stoffel et al.* [1991], and *Dragovich et al.* [2002]. Black dotted lines are magnetic lineaments from Figure 9. WRM, western Rattlesnake Mountain fault; MSB, Mount Stuart batholith; ML, Mount Lindsay structural zone; GR, Green River structural zone; WRF, White River fault; NRF, Naches River fault; CM, Cleman Mountain. See Figure 2 for other labels. (b) Aeromagnetic anomalies.

the Puget Lowland where considerable crustal earthquake activity is only approximately correlated with the numerous faults now mapped with confirmed Holocene displacement. Additional trenching on YFTB structures should clarify the late Quaternary/Holocene slip history and provide a basis for constructing an areal source zone similar to Puget Sound.

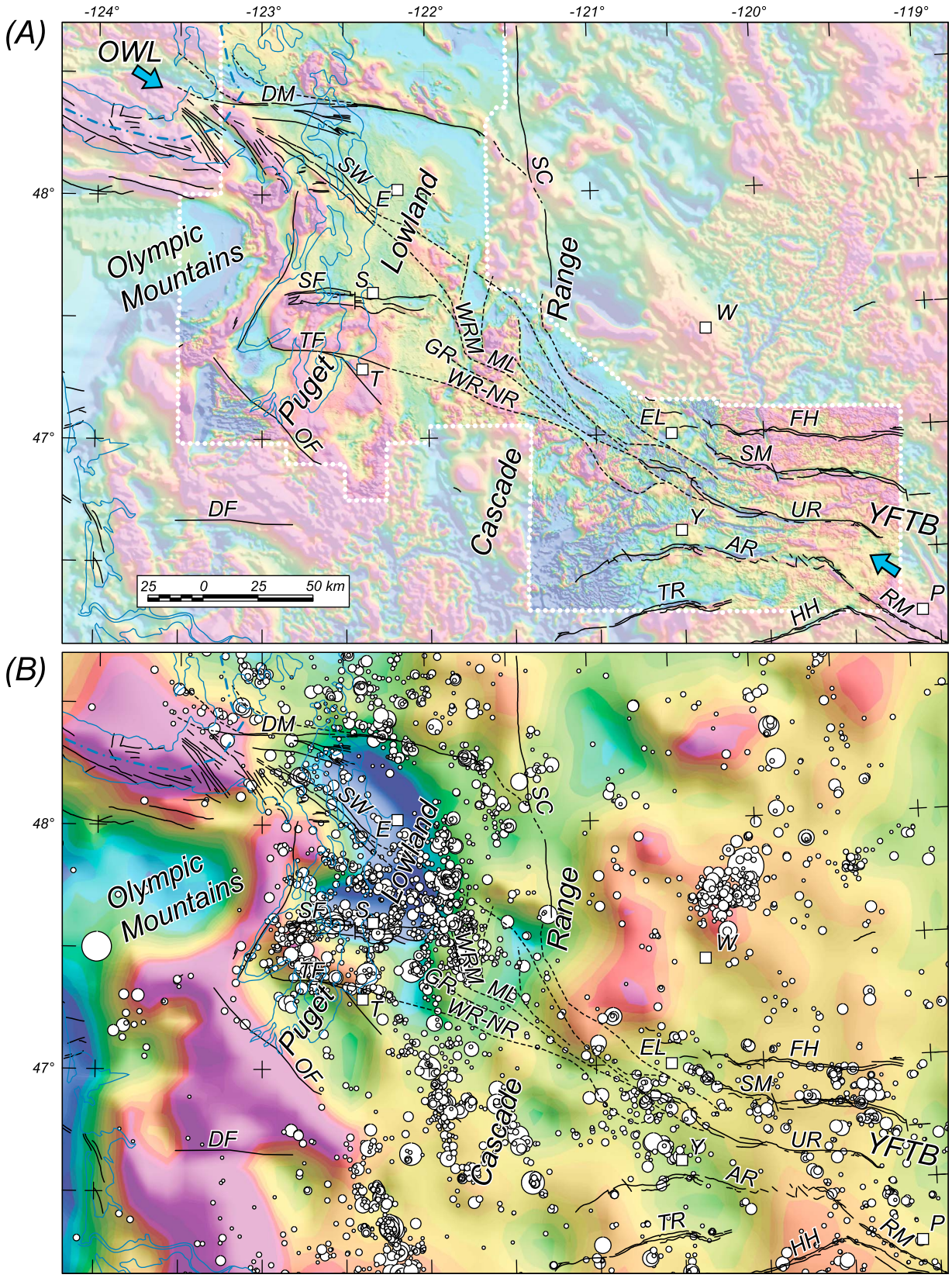

Figure 22

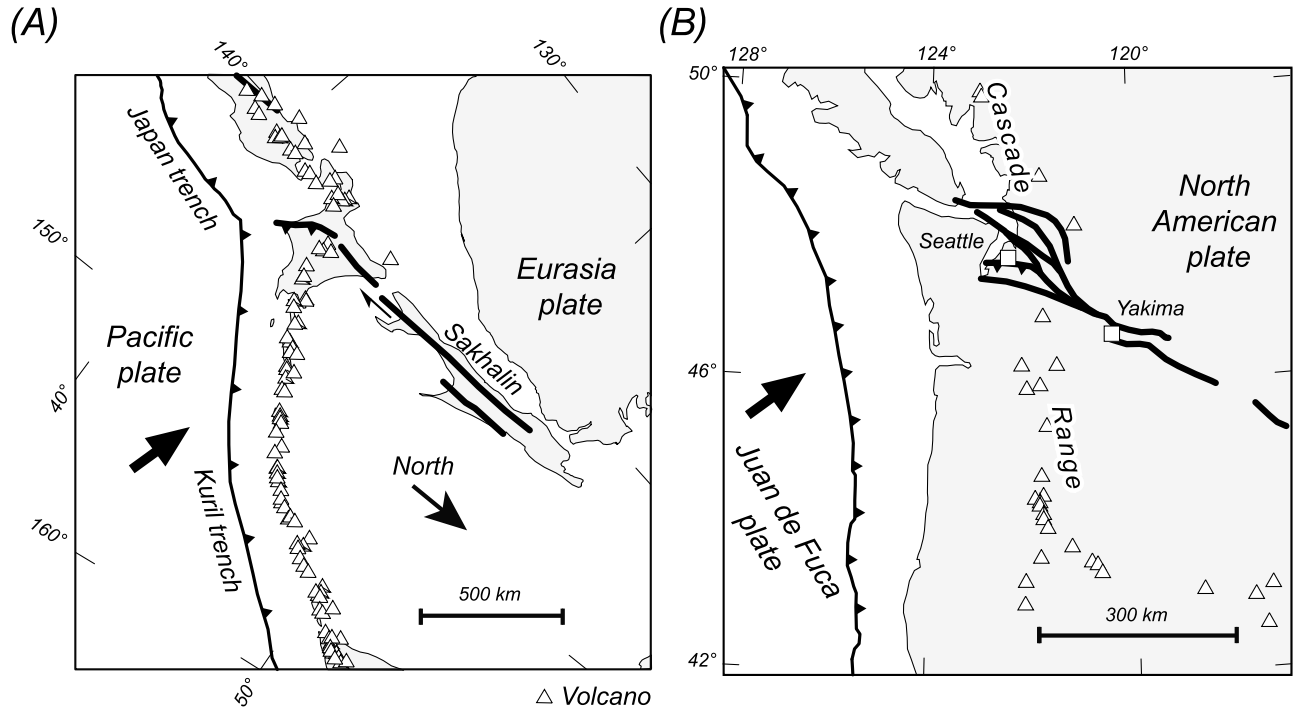

Figure 23. Comparison of the Sakhalin fault and the trans-Cascadia structural zone. (a) Japan-Kuril subduction zone. Map has been rotated so that trench is north-south for comparison with the accompanying Cascadia map. Triangles are Quaternary volcanoes. Bold arrow indicates motion of the Pacific plate relative to the Eurasian plate. Mapped location of Sakhalin fault from *Fournier et al.* [1994]. (b) Cascadia subduction zone. Note difference in scale between two maps.

[76] A second issue for earthquake hazard assessments is the potential length implied for mapped faults crossing the Cascade Range. Fault length is a fundamental measure of potential maximum magnitude on mapped crustal faults, and our model suggests that the Southern Whidbey Island fault is part of a continuous system that includes the western Rattlesnake Mountain and Umtanum Ridge faults (Figure 22). This trans-Cascadia system forms a fault zone over 200 km in length. Although it seems unlikely that earthquakes rupture the entire length of this structural zone, it does raise the possibility that the maximum magnitude used for hazard calculations for the Southern Whidbey Island fault, currently set at 7.44, will need adjustment as additional fieldwork is completed.

[77] Our interpretation of the Wooded Island earthquake swarm illustrates one advantage of using high-quality aeromagnetic surveys as the basis for exploring tectonic models and processes. Using aeromagnetic interpretations, we are able to track the Yakima Ridge southeastward beneath sedimentary cover toward the location of the earthquake swarm, suggesting that the swarm may be related to reactivated faults within the buried ridge. Without the ability to track the Yakima Ridge with aeromagnetic lineaments, it would be difficult to argue that one possibility for the swarm is related to major tectonic elements as opposed to hydrologic effects [*Wicks et al.*, 2009].

5.4. Analogs From Other Convergent Margins

[78] The model depicted in Figure 22 argues for a long-lived and currently active zone of faults linking the back arc and forearc of the Cascadia convergent margin in Washington. Similar structures are observed in other oblique subduction zones of the world, including the active Bio Bio and Gastre fault zones across the southern Andes [*Bohm et al.*, 2002], the transition from the Hikurangi subduction zone to the Alpine Fault system across New Zealand [*Furlong and Kamp*, 2009; *Eberhard-Phillips and Bannister*, 2010], and the Sakhalin fault across the island of Hokaido [*Fournier et al.*, 1994].

[79] Figure 23 illustrates similarities between the Sakhalin fault and the trans-Cascadia structure proposed here. Like Cascadia, the Japan-Kuril convergent margin is an oblique subduction zone, with the Pacific plate subducting obliquely beneath the Eurasia plate. Both the Sakhalin fault and the trans-Cascadia structure strike oblique to their respective arcs, extend from back-arc regions to across the arc, and upon entering the forearc rotate into trench-normal, com-

Figure 22. Interpretation of regional structures connecting Quaternary faults of the YFTB to active faults of the Puget Lowland. (a) Aeromagnetic anomalies. White dotted line indicates limit of high-resolution surveys discussed in this paper. Black solid lines are Quaternary faults (http://earthquake.usgs.gov/hazards/qfaults). Black dashed lines are interpreted structures. White dotted lines show limits of high-quality aeromagnetic data. Blue arrows indicate the Olympic-Wallowa lineament (OWL). See Figure 2 for label definitions. (b) Isostatic residual gravity anomalies and upper plate earthquakes, sized according to magnitude. See Figure 2 for magnitude scale.

pressional faults. Both structures have evolved since at least Miocene time and continue to be active today [*Fournier et al.*, 1994].

[80] Important differences between the Sakhalin and trans-Cascadia structures are also observed: the Sakhalin fault is 2000 km long [*Fournier et al.*, 1994], many times longer than the trans-Cascadia structure. The Sakhalin fault is largely a dextral strike-slip fault [*Fournier et al.*, 1994], whereas geologic arguments [e.g., *Reidel et al.*, 1989a] and GPS measurements [e.g., *McCaffrey et al.*, 2007] indicate that the trans-Cascadia structure is dominated by horizontal compression along most of its length and during most of its evolution.

6. Conclusions

[81] New aeromagnetic data from eastern Washington show the YFTB extending westward to beneath the Washington Cascade Range. Paleoseismic investigations demonstrate that at least one of the YFTB faults was active in Quaternary time, and diverse earthquake activity suggests that the region remains seismically active. We suggest that the Umtanum Ridge anticline splays into two structural zones that cross the Cascade Range. The southern zone, the White River–Naches River structural zone, may continue to the active Tacoma fault. The northern zone, the Mount Lindsay structural zone, links with the western Rattlesnake Mountain fault in the western Cascade Range foothills, which in turn links with the Southern Whidbey Island fault. Together these faults form a throughgoing structural zone extending from central Washington to the Olympic Peninsula. In the western YFTB, potential field data require dense basement rocks with greater relief than exhibited by deformed CRBG, suggesting that some faults in the YFTB penetrate pre-Tertiary basement.

[82] Thus, we suggest that faults and folds of the YFTB structurally connect with active faults in the Puget Sound. Puget Sound faults are known to have produced M6.5 to 7.0 earthquakes in Holocene time. Generally speaking, long faults are potentially more dangerous than short faults [*Wells and Coppersmith*, 1994], and the throughgoing faults proposed here would pose significantly increased seismic hazards if they should prove to be active along their entire lengths. Additional geologic and geophysical studies are needed, especially in the Cascade Range, to confirm and quantify their level of seismic potential.

[83] **Acknowledgments.** We thank Steve Reidel for providing borehole information and helpful comments. Discussions with Tom Sisson, Rowland Tabor, and Mike Sawlan helped clarify our thinking. Pat Hill, Eric Anderson, and Michelle Graham of the U.S. Geological Survey were instrumental in establishing contracts for the new aeromagnetic surveys. This manuscript greatly benefited from early reviews by Jon Hagstrum and Rick Saltus and from journal reviews by two anonymous reviewers.

References

Atwater, T. (1970), Implications of plate tectonics for the Cenozoic tectonic evolution of western North America, *Geol. Soc. Am. Bull.*, *81*, 3513–3536, doi:10.1130/0016-7606(1970)81[3513:IOPTFT]2.0.CO;2.

Beeson, M. H., T. L. Tolan, and J. L. Anderson (1989), The Columbia River Basalt Group in western Oregon; Geologic structures and other factors that controlled flow emplacement patterns, in *Volcanism and Tectonism in the Columbia River Flood-Basalt Province*, edited by S. P. Reidel and P. R. Hooper, *Spec. Pap. Geol. Soc. Am.*, *239*, 223–246.

Blakely, R. J. (1995), *Potential Theory in Gravity and Magnetic Applications*, 441 pp., Cambridge Univ. Press, New York, doi:10.1017/CBO9780511549816.

Blakely, R. J., R. E. Wells, and C. S. Weaver (1999), Puget Sound aeromagnetic maps and data, *U.S. Geol. Surv. Open File Rep.*, *1978*, 99–514. (Available at http://geopubs.wr.usgs.gov/open-file/of99-514.)

Blakely, R. J., R. E. Wells, C. S. Weaver, and S. Y. Johnson (2002), Location, structure, and seismicity of the Seattle fault zone, Washington: Evidence from aeromagnetic anomalies, geologic mapping, and seismic-reflection data, *Geol. Soc. Am. Bull.*, *114*, 169–177, doi:10.1130/0016-7606(2002)114<0169:LSASOT>2.0.CO;2.

Blakely, R. J., B. L. Sherrod, J. F. Hughes, M. L. Anderson, R. E. Wells, and C. S. Weaver (2009), Saddle Mountain fault deformation zone, Olympic Peninsula, Washington: Western boundary of the Seattle uplift, *Geosphere*, *5*, 105–125, doi:10.1130/GES00196.1.

Bohm, M., S. Lüth, H. Echtler, G. Asch, K. Bataille, C. Bruhn, A. Rietbrock, P. Wigger (2002), The southern Andes between 36° and 40°S latitude: Seismicity and average seismic velocities, *Tectonophysics*, *356*, 275–289, doi:10.1016/S0040-1951(02)00399-2.

Brocher, T. M., T. Parsons, R. J. Blakely, N. I. Christensen, M. A. Fisher, R. E. Wells, and the SHIPS Working Group (2001), Upper crustal structure in Puget Lowland, Washington: Results from 1998 Seismic Hazards Investigation in Puget Sound, *J. Geophys. Res.*, *106*, 13,541–13,564, doi:10.1029/2001JB000154.

Brocher, T. M., R. J. Blakely, and R. E. Wells (2004), Reinterpretation of the Seattle uplift, Washington, as a passive roof duplex, *Bull. Seismol. Soc. Am.*, *94*, 1379–1401, doi:10.1785/012003190.

Campbell, N. P. (1989), Structural and stratigraphic interpretation of rocks under the Yakima fold belt, Columbia Basin, based on recent surface mapping and well data, in *Volcanism and Tectonism in the Columbia River Flood-Basalt Province*, edited by S. P. Reidel and P. R. Hooper, *Spec. Pap. Geol. Soc. Am.*, *239*, 209–222.

Campbell, N. P., and R. D. Bentley (1981), Late Quaternary deformation of the Toppenish Ridge uplift in south-central Washington, *Geology*, *9*, 519–524, doi:10.1130/0091-7613(1981)9<519:LQDOTT>2.0.CO;2.

Catchings, R. D., and W. D. Mooney (1988), Crustal structure of the Columbia Plateau: Evidence for continental rifting, *J. Geophys. Res.*, *93*, 459–474, doi:10.1029/JB093iB01p00459.

Catchings, R. D., and R. W. Saltus (1994), Upper-crustal structure beneath the Columbia River Basalt Group, Washington: Gravity interpretation controlled by borehole and seismic studies: Discussion and reply, *Geol. Soc. Am. Bull.*, *106*, 1096–1105, doi:10.1130/0016-7606(1994)106<1096:UCSBTC>2.3.CO;2.

Cheney, E. S., and N. W. Hayman (2009), The Chiwaukum structural low: Cenozoic shortening of the central Cascade Range, Washington State, USA, *Geol. Soc. Am. Bull.*, *121*, 1135–1153, doi:10.1130/B26446.1.

Danes, Z. F., and W. M. Phillips (1983), Complete Bouguer gravity anomaly map, vol. 27, scale 1:250,000, Div. Geol. and Earth Res., Wash. Dept. Nat. Res., Olympia.

DeMets, C., R. G. Gordon, D. F. Argus, and S. Stein (1994), Effect of recent revisions to the geomagnetic reversal time scale on estimates of current plate motions, *Geophys. Res. Lett.*, *21*, 2191–2194, doi:10.1029/94GL02118.

Dragovich, J. D., R. L. Logan, H. W. Schasse, T. J. Walsh, W. S. Lingley Jr., D. K. Norman, W. J. Gerstel, T. J. Lapen, J. E. Schuster, and K. D. Meyers (2002), Geologic map of Washington—Northwest quadrant, *Geol. Map GM–50*, 72 pp., Div. Geol. and Earth Res., Wash. Dept. Nat. Res., Olympia.

Dragovich, J. D., H. A. Littke, M. L. Anderson, R. Hartog, G. R. Wessel, S. A. DuFrane, T. J. Walsh, J. H. MacDonald Jr., J. F. Mangano, and R. Caker (2009a), Geologic map of the Snoqualmie 7.5-minute quadrangle, King County, Washington, *Geol. Map GM–75*, scale 1:24,000, Div. Geol. and Earth Res., Wash. Dept. Nat. Res., Olympia.

Dragovich, J. D., et al. (2009b), Geologic map of the North Bend 7.5-minute quadrangle, King County, Washington, with a discussion of major faults, folds, and basins in the map area, *Geol. Map GM–73*, scale 1:24,000, Div. Geol. and Earth Res., Wash. Dept. Nat. Res., Olympia.

Eberhard-Phillips, D., and S. Bannister (2010), 3-D imaging of Marlborough, New Zealand, subducted plate and strike-slip systems, *Geophys. J. Int.*, *182*, 73–96, doi:10.1111/j.1365-246X.2010.04621.x.

Finn, C., K. C. Brenner, A. McCafferty, and R. Kucks (1989), Washington aeromagnetic maps and data, *U.S. Geol. Surv. Open File Rep.*, *1978*, 98–241.

Finn, C., W. M. Phillips, and D. L. Williams (1991), Gravity anomaly and terrain maps of Washington, scale 1:500000 and 1:1,000,000, *U.S. Geol. Surv. Geophys. Invest. Map, GP–988*.

Fournier, M., L. Jolivet, P. Huchon, K. F. Sergeyev, and L. S. Oscorbin (1994), Neogene strike-slip faulting in Sakhalin and the Japan Sea opening, *J. Geophys. Res.*, *99*, 2701–2725, doi:10.1029/93JB02026.

Frankel, A., C. Mueller, T. Barnhard, D. Perkins, E. Leyendecker, N. Dickman, S. Hanson, and M. Hopper (1996), National seismic-hazard maps—Documentation June 1996, *U.S. Geol. Surv. Open File Rep., 96–532*, 110 pp.

Frankel, A. D., et al. (2002), Documentation for the 2002 update of the national seismic hazard maps, *U.S. Geol. Surv. Open File Rep., 02–420*.

Furlong, K. P., and P. J. J. Kamp (2009), The lithospheric geodynamics of plate boundary transpression in New Zealand: Initiating and emplacing subduction along the Hikurangi margin, and the tectonic evolution of the Alpine Fault system, *Tectonophysics*, *474*, 449–462, doi:10.1016/j.tecto.2009.04.023.

Gresens, R. L., C. W. Naeser, and J. W. Whetten (1981), Stratigraphy and age of the Chumstick and Wenatchee Formations: Tertiary fluvial and lacustrine rocks, Chiwaukum graben, Washington, *Geol. Soc. Am. Bull.*, *92*, 223–236, doi:10.1130/0016-7606(1981)92<233:SAAOTC>2.0.CO;2.

Guffanti, M., and C. S. Weaver (1988), Distribution of late Cenozoic volcanic vents in the Cascade Range: Volcanic arc segmentation and regional tectonic considerations, *J. Geophys. Res.*, *93*, 6513–6529, doi:10.1029/JB093iB06p06513.

Haugerud, R. A., and R. W. Tabor (2009), Geologic map of the North Cascade Range, Washington, *U.S. Geol. Surv. Sci. Invest. Map 2940*, 23 pp.

Hooper, P. R., and R. M. Conrey (1989), A model for the tectonic setting of the Colmbia River basalt eruptions, in *Volcanism and Tectonism in the Columbia River Flood-Basalt Province*, edited by S. P. Reidel and P. R. Hooper, *Spec. Pap. Geol. Soc. Am.*, *239*, 293–306.

Jarchow, C. M. (1991), Investigations of magmatic underplating beneath the northwestern Basin and Range province, Nevada, seismic data acquisition and tectonic problems of the Columbia Plateau, Washington, and the nature of the Mohorovicic discontinuity worldwide, Ph.D. thesis, 258 pp., Stanford Univ., Stanford, Calif.

Johnson, S. Y., C. J. Potter, and J. M. Armentrout (1994), Origin and evolution of the Seattle Fault and Seattle Basin, Washington, *Geology*, *22*, 71–74, doi:10.1130/0091-7613(1994)022<0071:OAEOTS>2.3.CO;2.

Johnson, S. Y., C. J. Potter, J. M. Armentrout, J. J. Miller, C. A. Finn, and C. S. Weaver (1996), The Southern Whidbey Island Fault: An active structure in the Puget Lowland, Washington, *Geol. Soc. Am. Bull.*, *108*, 334–354, doi:10.1130/0016-7606(1996)108<0334:TSWIFA>2.3.CO;2.

Johnson, S. Y., et al. (2004a), Evidence for late Holocene earthquakes on the Utsalady Point Fault, northern Puget Lowland, Washington, *Bull. Seismol. Soc. Am.*, *94*, 2299–2316, doi:10.1785/0120040050.

Johnson, S. Y., R. J. Blakely, W. J. Stephenson, S. V. Dadisman, and M. A. Fisher (2004b), Active shortening of the Cascadia forearc and implications for seismic hazards of the Puget Lowland, *Tectonics*, *23*, TC1011, doi:10.1029/2003TC001507.

Kelsey, H. M., B. L. Sherrod, S. Y. Johnson, and S. V. Dadisman (2004), Land-level changes from a late Holocene earthquake in the northern Puget Lowland, Washington, *Geology*, *32*, 469–472, doi:10.1130/G20361.1.

Kelsey, H. M., B. L. Sherrod, A. R. Nelson, and T. M. Brocher (2008), Earthquakes generated from bedding plane-parallel reverse faults above an active wedge thrust, Seattle fault zone, *Geol. Soc. Am. Bull.*, *120*, 1581–1597, doi:10.1130/B26282.1.

Kienle, C. F., Jr., R. D. Bentley, and J. L. Anderson (1977), Geologic reconnaissance of the Cle Elum-Wallula lineament and related structures, in *Washington Public Power Supply System PSAR and WPPSS Nuclear Projects 1 and 4*, Amendment 23, 33 pp., Shannon and Wilson, Inc., Seattle, Wash.

MacQueen, J. D., and E. Mann (2007), Borehole gravity meter surveys at the waste treatment plant, Hanford, Washington, *Rep. PNNL–16490*, 26 pp., Pac. Northwest Natl. Lab., Richland, Wash.

Mattinson, J. M. (1977), Emplacement history of the Tatoosh volcanic-plutonic complex, Washington: Ages of zircons, *Geol. Soc. Am. Bull.*, *88*, 1509–1514, doi:10.1130/0016-7606(1977)88<1509:EHOTTV>2.0.CO;2.

Mazzotti, S., H. Dragert, R. D. Hyndman, M. M. Miller, and J. A. Henton (2002), GPS deformation in a region of high crustal seismicity: N. Cascadia forearc, *Earth Planet. Sci. Lett.*, *198*, 41–48, doi:10.1016/S0012-821X(02)00520-4.

McCaffrey, R., M. Long, C. Goldfinger, P. C. Zwick, J. L. Nabelek, C. K. Johnson, and C. Smith (2000), Rotation and plate locking at the southern Cascadia subduction zone, *Geophys. Res. Lett.*, *27*, 3117–3120, doi:10.1029/2000GL011768.

McCaffrey, R., A. I. Qamar, R. W. King, R. Wells, G. Khazaradze, C. A. Williams, C. W. Stevens, J. J. Vollick, and P. C. Zwick (2007), Fault locking, block rotation and crustal deformation in the Pacific Northwest, *Geophys. J. Int.*, *169*(3), 1315–1340, doi:10.1111/j.1365-246X.2007.03371.x.

Mitchell, S. G., and D. R. Montgomery (2006), Polygenetic topography of the Cascade Range, Washington State, USA, *Am. J. Sci.*, *306*, 736–768, doi:10.2475/09.2006.03.

Nelson, A. R., S. Y. Johnson, H. M. Kelsey, R. E. Wells, B. L. Sherrod, S. K. Pezzopane, L.-A. Bradley, R. D. Koehler III, and R. C. Bucknam (2003), Late Holocene earthquakes on the Toe Jam Hill fault, Seattle fault zone, Bainbridge Island, Washington, *Geol. Soc. Am. Bull.*, *115*, 1388–1403, doi:10.1130/B25262.1.

Parker, R. L. (1972), The rapid calculation of potential anomalies, *Geophys. J. R. Astron. Soc.*, *31*, 447–455.

Petersen, M. D., et al. (2008), Documentation for the 2008 update of the United States national seismic hazard maps, *U.S. Geol. Surv. Open File Rep., 2008–1128*, 61 pp.

Phillips, J. D., R. O. Hansen, and R. J. Blakely (2007), The use of curvature in potential-field interpretation, *Explor. Geophys.*, *38*, 111–119, doi:10.1071/EG07014.

Pratt, T. L., S. Johnson, C. Potter, W. Stephenson, and C. Finn (1997), Seismic reflection images beneath Puget Sound, western Washington State: The Puget lowland thrust sheet hypothesis, *J. Geophys. Res.*, *102*, 27,469–27,489, doi:10.1029/97JB01830.

Price, E. E., and A. J. Watkinson (1989), Structural geometry and strain distribution within eastern Umtanum fold ridge, south-central Washington, in *Volcanism and Tectonism in the Columbia River Flood-Basalt Province*, edited by S. P. Reidel and P. R. Hooper, *Spec. Pap. Geol. Soc. Am.*, *239*, 265–281.

Raisz, E. (1945), The Olympic-Wallowa lineament, *Am. J. Sci.*, *243*, 479–485.

Reidel, S. P. (1984), The Saddle Mountains: The evolution of an anticline in the Yakima fold belt, *Am. J. Sci.*, *284*, 942–978, doi:10.2475/ajs.284.8.942.

Reidel, S. P., K. R. Fecht, M. C. Hagood, and T. L. Tolan (1989a), The geologic evolution of the central Columbia Plateau, in *Volcanism and Tectonism in the Columbia River Flood-Basalt Province*, edited by S. P. Reidel and P. R. Hooper, *Spec. Pap. Geol. Soc. Am.*, *239*, 247–264.

Reidel, S. P., T. L. Tolan, P. R. Hooper, M. H. Beeson, K. R. Fecht, and J. L. Anderson (1989b), The Grande Ronde Basalt, Columbia River Basalt Group; Stratigraphic descriptions and correlations in Washington, Oregon, and Idaho, in *Volcanism and Tectonism in the Columbia River Flood-Basalt Province*, edited by S. P. Reidel and P. R. Hooper, *Spec. Pap. Geol. Soc. Am.*, 239, 21–53.

Reidel, S. P., N. P. Campbell, K. R. Fecht, and K. A. Lindsey (1994), Late Cenozoic structure and stratigraphy of south-central Washington, in *Regional Geology of Washington State*, *Wash. Div. Geol. Earth Resour. Bull.*, 80, 159–180.

Reiners, P. W., T. A. Ehlers, J. I. Garver, S. G. Mitchell, D. R. Montgomery, J. A. Vance, and S. Nicolescu (2002), Late Miocene exhumation and uplift of the Washington Cascade Range, *Geology*, *30*, 767–770, doi:10.1130/0091-7613(2002)030<0767:LMEAUO>2.0.CO;2.

Repasky, T. R., E. R. Hyde, C. A. Link, and M. A. Speece (2009), Landstreamer/gimbaled geophone acquisition of high-resolution seismic reflection data north of the 200 Areas, Hanford Site, *Rep. SGW–43746*, 78 pp., U.S. Dep. of Energy, Washington, D. C.

Robbins, S. L., R. J. Martinez, and D. L. Smith (1979), Principal facts for borehole gravity stations in wells DC–3, DC–5, DC–7 at the Hanford site, Washington, and in well RSH#1 on Rattlesnake Hills, *U.S. Geol. Surv. Open File Rep., 79–849*, 27 pp.

Roberts, C. W., R. J. Blakely, and C. Finn (1997), Preliminary merged aeromagnetic map of Oregon, *U.S. Geol. Surv. Open File Rep., 97–0440*.

Rohay, A. (2009), Ground motion amplitudes from the Wooded Island earthquake swarm, Hanford, Washington, *Eos Trans. AGU*, *90*(52), Fall Meet. Suppl., Abstract S41F–05.

Saltus, R. W. (1993), Upper-crustal structure beneath the Columbia River Basalt Group, Washington: Gravity interpretation controlled by borehole and seismic studies, *Geol. Soc. Am. Bull.*, *105*, 1247–1259, doi:10.1130/0016-7606(1993)105<1247:UCSBTC>2.3.CO;2.

Schuster, J. E. (1994), Geologic map of the east half of the Yakima 1:100,000 quadrangle, Washington, *Open File Rep. 94–12*, Wash. Div. of Geol. and Earth Resour., 19 pp.

Schuster, J. E., C. W. Gulick, S. P. Reidel, K. R. Fecht, and S. Zurenko (1997), Geologic map of Washington—Southeast quadrant (1997), *Geol. Map GM–45*, 20 pp., Div. Geol. and Earth Res., Wash. Dept. Nat. Res., Olympia.

Sherrod, B. L., T. M. Brocher, C. S. Weaver, R. C. Bucknam, R. J. Blakely, H. M. Kelsey, A. R. Nelson, and R. A. Haugerud (2004), Holocene fault scarps near Tacoma, Washington, *Geology*, *32*, 9–12, doi:10.1130/G19914.1.

Sherrod, B. L., R. J. Blakely, C. S. Weaver, H. M. Kelsey, E. Barnett, L. Liberty, K. L. Meagher, and K. Pape (2008), Finding concealed active faults: Extending the Southern Whidbey Island fault across the Puget Lowland, Washington (2008), *J. Geophys. Res.*, *113*, B05313, doi:10.1029/2007JB005060.

Simpson, R. W., and A. Cox (1977), Paleomagnetic evidence for tectonic rotation of the Oregon Coast Range, *Geology*, *5*, 585–589, doi:10.1130/0091-7613(1977)5<585:PEFTRO>2.0.CO;2.

Simpson, R. W., R. C. Jachens, R. J. Blakely, and R. W. Saltus (1986), A new isostatic residual gravity map of the conterminous United States with a discussion of the significance of isostatic residual anomalies, *J. Geophys. Res.*, *91*, 8348–8372, doi:10.1029/JB091iB08p08348.

Smith, G. O. (1904), *Mount Stuart Folio, Geologic Atlas of the United States*, vol. 106, 10 pp., U.S. Geol. Surv., Reston, Va.

Stoffel, K. L., N. L. Joseph, S. Z. Waggoner, C. W. Gulick, M. A. Korosec, and B. B. Bunning (1991), Geologic map of Washington—Northeast quadrant, *Geol. Map GM–34*, 36 pp., Div. Geol. and Earth Res., Wash. Dept. Nat. Res., Olympia.

Swanson, D. A., T. L. Wright, and I. Zietz (1979), Aeromagnetic map and geologic interpretation of the west-central Columbia Plateau, Washington and Oregon, scale 1:250,000, *U.S. Geol. Surv. Geophys. Map 917*.

Tabor, R. W., V. A. Frizzell Jr., J. A. Vance, and C. W. Naeser (1984), Ages and stratigraphy of lower and middle Tertiary sedimentary and volcanic rocks of the central Cascades, Washington: Application to the tectonic history of the Straight Creek fault, *Geol. Soc. Am. Bull.*, *95*, 26–44, doi:10.1130/0016-7606(1984)95<26:AASOLA>2.0.CO;2.

Tabor, R. W., V. A. Frizzell Jr., D. B. Booth, and R. B. Waitt (2000), Geologic map of the Snoqualmie Pass 30′ × 60′ quadrangle, Washington, scale 1:100,000, *U.S. Geol. Surv. Geol. Invest. Series Map I-2538*.

ten Brink, U. S., P. C. Molzer, M. A. Fisher, R. J. Blakely, R. C. Bucknam, T. Parsons, R. S. Crosson, and K. C. Creager (2002), Subsurface geometry and evolution of the Seattle fault zone and the Seattle basin, *Bull. Seismol. Soc. Am.*, *92*, 1737–1753, doi:10.1785/0120010229.

Thelen, W. A., J. S. Gomberg, P. Bodin, R. Hartog, A. Wright, and A. Rohay (2009), A tale of two seismic swarms: Implications for different forcing mechanisms, *Eos Trans. AGU*, *90*(52), Fall Meet. Suppl., Abstract S41F–03.

Thorne, P. D., M. P. Bergeron, M. D. Williams, and V. L. Freedman (2006), Groundwater data package for Hanford assessments, *Rep. PNNL–14753*, 13,787 pp., Pac. Northwest Natl. Lab., Richland, Wash.

Tolan, T. L., and S. P. Reidel (1989), Structure map of a portion of the Columbia River flood-basalt province, in *Volcanism and Tectonism in the Columbia River Flood-Basalt Province*, edited by S. P. Reidel and P. R. Hooper, *Spec. Pap. Geol. Soc. Am.*, *239*, Plate 1.

Tolan, T. L., S. P. Reidel, M. H. Beeson, J. L. Anderson, K. R. Fecht, and D. A. Swanson (1989), Revisions to the estimates of the areal extent and volume of the Columbia River Basalt Group, in *Volcanism and Tectonism in the Columbia River Flood-Basalt Province*, edited by S. P. Reidel and P. R. Hooper, *Spec. Pap. Geol. Soc. Am.*, *239*, pp. 1–20.

Tolan, T. L., B. S. Martin, S. P. Reidel, J. L. Anderson, K. A. Lindsey, and W. Burt (2009), An introduction to the stratigraphy, structural geology, and hydrogeology of the Columbia River Flood-Basalt Province: A primer for the GSA Columbia River Basalt Group field trips, in *Volcanoes to Vineyards—Geologic Field Trips Through the Dynamic Landscape of the Pacific Northwest*, edited by J. E. O'Connor, R. J. Dorsey, and I. P. Madin, *Geol. Soc. Am. Field Guide*, *15*, 599–643, doi:10.1130/2009.fld015(28).

Waitt, R. W. (1979), Late-Cenozoic deposits, landforms, stratigraphy, and tectonism of Kittitas Valley, Washington, *U.S. Geol. Surv. Prof. Pap., 1127*, 18 pp.

Walsh, T. J., M. A. Korosec, W. M. Phillips, R. L. Logan, and H. W. Schasse (1987), Geologic map of Washington—Southwest quadrant, *Geol. Map GM–34*, 28 pp., Div. Geol. and Earth Res., Wash. Dept. Nat. Res., Olympia.

Wells, D. L., and K. J. Coppersmith (1994), New empirical relationships among magnitude, rupture length, rupture width, rupture area, and surface displacement, *Bull. Seismol. Soc. Am.*, *84*, 974–1002.

Wells, R. E. (1990), Paleomagnetic rotations and the Cenozoic tectonics of the Cascade arc, Washington, Oregon, and California, *J. Geophys. Res.*, *95*, 19,409–19,417, doi:10.1029/JB095iB12p19409.

Wells, R. E., C. S. Weaver, and R. J. Blakely (1998), Fore-arc migration in Cascadia and its neotectonic significance, *Geology*, *26*, 759–762, doi:10.1130/0091-7613(1998)026<0759:FAMICA>2.3.CO;2.

Wells, R. E., A. R. Niem, R. C. Evarts, and J. T. Hagstrum (2009), The Columbia River Basalt Group from the gorge to the sea, in *Volcanoes to Vineyards—Geologic Field Trips Through the Dynamic Landscape of the Pacific Northwest*, edited by J. E. O'Connor, R. J. Dorsey, and I. P. Madin, *Geol. Soc. Am. Field Guide*, *15*, 737–774, doi:10.1130/2009.fld015(32).

West, M. W., F. X. Ashland, A. J. Busacca, G. W. Berger, and M. E. Shaffer (1996), Late Quaternary deformation, Saddle Mountains anticline, south-central Washington, *Geology*, *24*, 1123–1126, doi:10.1130/0091-7613(1996)024<1123:LQDSMA>2.3.CO;2.

Weston Geophysical Research (1977), Evaluation of microearthquake activity in eastern Washington, WNP–1/4 PSAR, Amendment, 23 (Appendix), 2RJ., Wash. Pub. Supply Syst., Richland, Wash.

Wicks, C. W., J. S. Gomberg, and C. S. Weaver (2009), InSAR measurement of surface deformation at the Hanford Reservation associated with the 2009 Wooded Island earthquake swarm, *Eos Trans. AGU*, *90*(52), Fall Meet. Suppl., Abstract S41F–04.

Yeats, R. S. (1986), Active faults related to folding, in *Active Tectonics*, pp. 80–94, National Acad. Press, Washington, D. C.

E. A. Barnett, B. L. Sherrod, and C. S. Weaver, U.S. Geological Survey at Department of Earth and Space Sciences, University of Washington, Seattle, WA 98195, USA.

R. Blakely, N. E. Knepprath, and R. E. Wells, U.S. Geological Survey, 345 Middlefield Rd., Menlo Park, CA 94025, USA. (blakely@usgs.gov)

A. C. Rohay, Environmental Characterization and Risk Assessment Group, Pacific Northwest National Laboratory, PO Box 999, Richland, WA 99352, USA.